# REPORT DOCUMENTATION PAGE

Form Approved
OMB No 0704-0188





| 2. REPORT DATE | 3. REPORT TYPE AND DATES COVERED |
|---|---|
| January 14, 1991 | Final Technical Report 1989-90 |

**4. TITLE AND SUBTITLE**
DN Hard Materials Laser Assisted Formation of Dense Phases

**5. FUNDING NUMBERS**
N00014-89-J-3092

**6. AUTHOR(S)**
Rustum Roy (many co-authors)



**7. PERFORMING ORGANIZATION NAME(S) AND ADDRESS(ES)**
The Pennsylvania State University
Materials Research Laboratory
University Park, PA 16802

**PERFORMING ORGANIZATION REPORT NUMBER**

**9. SPONSORING / MONITORING AGENCY NAME(S) AND ADDRESS(ES)**
Norman A. Meeks, Administrative Contracting Officer
Resident Representative N66005, ONR
The Ohio State University Research Center
1314 Kinnear Road
Columbus, OH 43212-1194

**10. SPONSORING / MONITORING AGENCY REPORT NUMBER**

**11. SUPPLEMENTARY NOTES**
The report includes many reprints by different colleagues who cooperated in the work.

**12a. DISTRIBUTION / AVAILABILITY STATEMENT**
No restrictions.





**13. ABSTRACT** *(Maximum 200 words)*

Diamond and other high-pressure phases of carbon were synthesized in air by exposing fine particles of carbon black to carbon dioxide and Nd-YAG laser radiation. The high-pressure phases were separated from the carbon black by selective oxidation and were characterized by electron and x-ray diffraction. Formation of cubic diamond, chaoite, and graphite was confirmed.

Exposure of a falling stream of 1 μm average size α-quartz particles to a continuous wave or pulsed $CO_2$ laser beam in air resulted in the formation of a complete series of high-pressure phases of silica: coesite, stishovite, and apparently even denser forms with α-$PbO_2$ and $Fe_2N$ structures. Since the laser exposure technique works with the carbon black to diamond trannsition, the technique is confirmed as a simple and generally applicable means to achieve the same effects as exposure to several hundred kilobars pressure.

High-pressure phases of $CaCO_3$, namely aragonite, calcite II, and possibly calcite III, were synthesized in air by exposing 10- to 20-μm-size particles of $CaCO_3$ (calcite I phase) to a $CO_2$ laser radiation at short pulse lengths (≤0.1 ms).

The system B-O was explored at high pressures and some very interesting new materials prepared near the composition $B_{12}O$-$B_{22}O$. The properties were *not* reproducible.

| 14. SUBJECT TERMS | 15. NUMBER OF PAGES |
|---|---|
| Diamond synthesis via laser pulses, Novel hard $B_xO$ phases | 16. PRICE CODE |

| 17. SECURITY CLASSIFICATION OF REPORT | 18. SECURITY CLASSIFICATION OF THIS PAGE | 19. SECURITY CLASSIFICATION OF ABSTRACT | 20. LIMITATION OF ABSTRACT |
|---|---|---|---|
| unclassified | unclassified | unclassified | UL |

NSN 7540-01-280-5500

Standard Form 298 (Rev. 2-89)
Prescribed by ANSI Std. Z39-18
298-102

## GENERAL INSTRUCTIONS FOR COMPLETING SF 298

The Report Documentation Page (RDP) is used in announcing and cataloging reports. It is important that this information be consistent with the rest of the report, particu .ly the cover and title page. Instructions for filling in each block of the form follow. It is important to ***stay within the lines*** to meet ***optical scanning requirements***.

**Block 1.** Agency Use Only *(Leave blank)*

**Block 2.** Report Date. Full publication date including day, month, and year, if available (e.g. 1 Jan 88). Must cite at least the year.

**Block 3.** Type of Report and Dates Covered. State whether report is interim, final, etc. If applicable, enter inclusive report dates (e.g. 10 Jun 87 - 30 Jun 88).

**Block 4.** Title and Subtitle. A title is taken from the part of the report that provides the most meaningful and complete information. When a report is prepared in more than one volume, repeat the primary title, add volume number, and include subtitle for the specific volume. On classified documents enter the title classification in parentheses.

**Block 5.** Funding Numbers. To include contract and grant numbers; may include program element number(s), project number(s), task number(s), and work unit number(s). Use the following labels:

| | | | |
|---|---|---|---|
| C | - Contract | PR | - Project |
| G | - Grant | TA | - Task |
| PE | - Program Element | WU | - Work Unit Accession No. |

**Block 6.** Author(s). Name(s) of person(s) responsible for writing the report, performing the research, or credited with the content of the report. If editor or compiler, this should follow the name(s).

**Block 7.** Performing Organization Name(s) and Address(es). Self-explanatory.

**Block 8.** Performing Organization Report Number. Enter the unique alphanumeric report number(s) assigned by the organization performing the report.

**Block 9.** Sponsoring/Monitoring Agency Name(s) and Address(es). Self-explanatory.

**Block 10.** Sponsoring/Monitoring Agency Report Number. *(If known)*

**Block 11.** Supplementary Notes. Enter information not included elsewhere such as: Prepared in cooperation with...; Trans. of...; To be published in... When a report is revised, include a statement whether the new report supersedes or supplements the older report.

**Block 12a.** Distribution/Availability Statement. Denotes public availability or limitations. Cite any availability to the public. Enter additional limitations or special markings in all capitals (e.g. NOFORN, REL, ITAR).

- **DOD** - See DoDD 5230.24, "Distribution Statements on Technical Documents."
- **DOE** - See authorities.
- **NASA** - See Handbook NHB 2200.2.
- **NTIS** - Leave blank.

**Block 12b.** Distribution Code.

- **DOD** - Leave blank.
- **DOE** - Enter DOE distribution categories from the Standard Distribution for Unclassified Scientific and Technical Reports.
- **NASA** - Leave blank.
- **NTIS** - Leave blank.

**Block 13.** Abstract. Include a brief *(Maximum 200 words)* factual summary of the most significant information contained in the report.

**Block 14.** Subject Terms. Keywords or phrases identifying major subjects in the report.

**Block 15.** Number of Pages. Enter the total number of pages.

**Block 16.** Price Code. Enter appropriate price code *(NTIS only)*.

**Blocks 17. - 19.** Security Classifications. Self-explanatory. Enter U.S. Security Classification in accordance with U.S. Security Regulations (i.e., UNCLASSIFIED). If form contains classified information, stamp classification on the top and bottom of the page.

**Block 20.** Limitation of Abstract. This block must be completed to assign a limitation to the abstract. Enter either UL (unlimited) or SAR (same as report). An entry in this block is necessary if the abstract is to be limited. If blank, the abstract is assumed to be unlimited.

# DISCLAIMER NOTICE

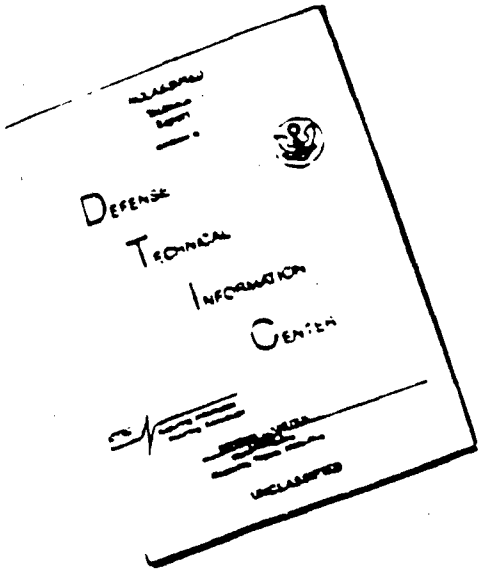


THIS DOCUMENT IS BEST QUALITY AVAILABLE. THE COPY FURNISHED TO DTIC CONTAINED A SIGNIFICANT NUMBER OF PAGES WHICH DO NOT REPRODUCE LEGIBLY.

# SYNTHESIS OF HARD MATERIALS BY LASER PROCESS AND IN B-O SYSTEM

## SUMMARY OF RESEARCH

As indicated in the proposed work for the contract, we followed two areas in parallel:

1. Laser-assisted synthesis of high density phases including $CaCO_3$;
2. New "ultrahard" phases in the system B-O.

This ONR grant can take credit for establishing the laser route to hard materials as a reality for the world which did not believe the Derjaguin results. our work not only confirmed their work but extended it into novel composition ($CaCO_3$) to explain its mechanism. Today there is a sudden burst of interest in the process from India to Japan. The abstracts of our five papers in the field give a useful summary of our achievements.

1. Diamond Formation in Air by the Fedoseev-Derjaguin Laser Process

   Diamond and other high-pressure phases of carbon were synthesized in air by exposing fine particles of carbon black to carbon dioxide and Nd-YAG laser radiation. The high-pressure phases were separated from the carbon black by selective oxidation and were characterized by electron and x-ray diffraction. Formation of cubic diamond, chaoite, and graphite were confirmed.

2. High-Pressure Phases of $SiO_2$ Made in Air by Fedoseev-Derjaguin Laser Process

   Exposure of a falling stream of 1μm average size α-quartz particles to a continuous wave or pulsed $CO_2$ laser beam in air resulted in the formation of a complete series of high-pressure phases of silica: coesite, stishovite, and apparently even denser forms with α-$PbO_2$ and $Fe_2N$ structures. Since the laser exposure technique works with the carbon black to diamond transition, the technique is confirmed as a simple and generally applicable means to achieve the same effects as exposure to several hundred kilobars pressure.

3. TEM Characterization of Structural Changes in Graphite Plates due to Pulsed $CO_2$ Laser Irradiation

4. Separation of Synthetic Diamond from Carbon Black by Oxidation

5. Laser-Induced Calcite-Aragonite Transition

   High-pressure phases of $CaCO_3$, namely aragonite, calcite II, and possibly calcite III, were synthesized in air by exposing 10- to 20-mm-size particles of $CaCO_3$ (calcite I phase) to a $CO_2$ laser radiation at short pulse lengths (≤0.1 ms). The process, therefore, has the same effect as exposing the particles to at least several hundred megapascals pressure. Processing at higher pulse lengths resulted in the decomposition of $CaCO_3$ to CaO and $CO_2$. The extent of decomposition increased with increasing pulse length.

The papers themselves are appended to provide full details on our work.

The $B_xO$ work also has stirred up interest worldwide but it was much less definitive. Clearly there is something there! There appears to be a unique, very hard phase which scratches diamond. The data from Oxford University illustrate the problem—extremely high hardness numbers in one part of the sample and very modest in others.

One abstract follows:

1. $B_xO$; Phases Present at High Pressure and Temperature

   Boron suboxide compounds are of interest because of their low densities coupled with high hardness. In the present study, we have attempted to determine the nature of the $B_xO$ phases that occur in the field defined by pressures of zero to 1.5 GPa, temperature between 1200° and 1700°C, and the compositional range $2/3 \leq x \leq 24$. Amorphous boron powder and boric acid $B_2O_3$ were the starting reactants for all the runs. The processing of the specimens was carried out in a controlled atmosphere furnace, a hot pressing assembly and in a piston-cylinder high pressure apparatus within quasi-hydrostatic and inductively heated cell assemblies. After processing at elevated temperature and pressure, for compositions over the range $2/3 \leq x \leq 6$, $B_2O_3$ (identical to the hexagonal starting material) and $B_6O$ ($R\bar{3}m$) were the dominant phases present. For the compositions $7 \leq x \leq 24$, $B_6O$ and rhombohedral B were the primary phases identified. In general, the hardness of the processed composites was dominated by the occurrence of $B_6O$ (approximately equivalent to $B_4C$). However, there is some suggestion of particularly high values of hardness on a very localized scale in specimens near the $B_{22}O$ composition.

The conclusion is obvious: There is much to be gained from *high-risk* research in the diamond field.

Carbon Vol 27, No. 2, pp. 289–294, 1989
Printed in Great Britain.

0008-6223/89 $3.00 + .00


# DIAMOND FORMATION IN AIR BY THE FEDOSEEV–DERJAGUIN LASER PROCESS

M. ALAM, T. DEBROY, R. ROY, and E. BREVAL
Materials Research Laboratory, The Pennsylvania State University, University Park, PA 16802

(*Received* 27 *July* 1988; *accepted in revised form* 10 *October* 1988)

**Abstract**—Diamond and other high-pressure phases of carbon were synthesized in air by exposing fine particles of carbon black to carbon dioxide and Nd-YAG laser radiation. The high-pressure phases were separated from the carbon black by selective oxidation and were characterized by electron and x-ray diffraction. Formation of cubic diamond, chaoite, and graphite was confirmed.

**Key Words**—Diamond, laser radiation, Derjaguin, chaoite.

## 1. INTRODUCTION

Diamond is widely used as hard coatings for cutting and grinding tools, as films in semiconductor devices, and in optical and audio components. Work on the synthesis of diamond was initiated several decades ago. Much of the previous work was concerned with the transformation of various carbonaceous materials to synthetic diamond by application of high pressure and temperature where diamond is the thermodynamically stable form. Examples of successful diamond synthesis by application of static pressure include the General Electric process[1], the work of Liander and Lundblad[2], Bundy[3] and Vereshchagin *et al.*[4]. In experiments conducted by DeCarli and Jameison[5] and in the DuPont process[6] high dynamic pressures were applied to carbon samples by detonation of suitable explosives to yield diamonds. Today, diamond films are being grown from hydrogen–hydrocarbon mixtures at less than atmospheric pressure and at temperatures below 1000°C by plasma-assisted vapor deposition techniques[7–11] based on work done mainly in the USSR[7] and later in Japan[10].

In 1983 Fedoseev and Derjaguin[12,13] reported a radically different and incredibly simple method of diamond synthesis. The technique involved exposing a flowing loose powder of carbon black, in air, to a modest carbon dioxide laser flux, 1500 watts/cm² in continuous wave mode. They claimed that this simple treatment resulted in the transformation of fine carbon black particles to high-pressure phases like α and β carbynes, chaoite, lonsdaleite, and diamond. The separation of the transformed high-pressure phases from the untransformed carbon black was not easy. It involved boiling of the laser-treated material in hydrochloric acid for 10 h and subsequent oxidation in air plasma at 100°C. Although their work opened up a potentially new technique for the synthesis of high-pressure phases, an enormous range of important questions remain unanswered. How generalizable is the process? Can the increase in power density or change in laser wavelength lead to a better yield of material? Can the diamond be separated by a relatively simple technique?

The objective of this work was to confirm and extend the works of Fedoseev *et al.*[12,13]. In the experiments reported in this article the variables studied were the power density, wavelength of laser, and the laser mode (continuous wave and pulsed). Finely divided α-quartz particles were also exposed to the laser beam to examine the generality of the process[14].

If, indeed, the mere exposure to high fluxes of photons can cause *solid state* transformations, the method becomes a general tool in materials science. Understanding the mechanism offers a challenge and an opportunity to extend its use as a synthetic tool which could possibly produce phases unattainable by other means. The implications for theories of cosmology and stellar and planetary formation could also be far-reaching.

## 2. EXPERIMENTAL

A variety of carbon black and graphite particles were selected ranging in size from 20 to 1000 nm. Streams of such particles were exposed to both continuous wave and pulsed $CO_2$ and Nd-YAG laser beams at various power densities. The processed material was concentrated to separate the high-pressure product phases from the untransformed material and analyzed by x-ray and electron diffraction for the identification of the products. A schematic diagram of the experimental set-up is shown in Fig. 1. The set-up consisted of either an Everlase model 525 $CO_2$ laser or a Raytheon Nd-YAG laser and an electrically powered vibrating feeder. The particles were injected horizontally and were treated with a vertically transmitted laser beam. The laser-processed particles were collected in a glass beaker.

The discharge from the powder feeder was suitably positioned such that the particles could interact with the laser beam either at the focal spot or at a

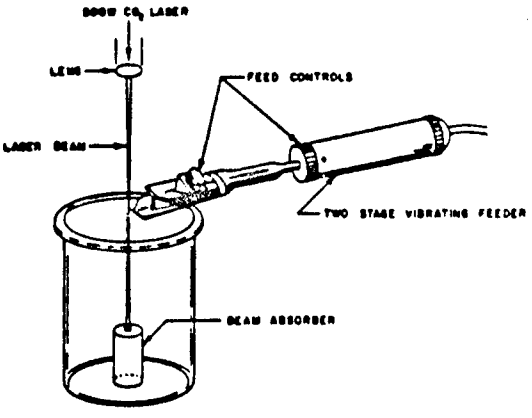


Fig. 1. Schematic diagram of the experimental set-up.

predetermined distance from the focal spot. The laser-treated material was recycled several times to ensure improved laser-particle interaction. The types of materials used and the specific conditions of the experiments are given in Table 1.

The laser-treated samples were partly oxidized in order to enr'·h the denser product phase. The kinetics of oxidation of carbon black in air at 773 K were found to be much faster than for diamond. The details of the selective oxidation work were recently reported[15] in *Carbon*. The laser-processed samples were heated in air for at least 16,600 s. The portion of the samples recovered after the oxidation treatment was dispersed in a bromoform-acetone solution of density 2.40 gm/cc. Since the respective densities of carbon black and diamond are 2.05 gm/cc and 3.52 gm/cc, only particles containing at least 25% diamond by volume could settle. The dense fraction was then analyzed by x-ray and electron diffraction.

## 3. RESULTS AND DISCUSSION

Untreated and laser-treated carbon black samples after enrichment were analyzed by electron diffraction for the identification of various carbon forms. The unprocessed carbon black particles were amorphous and those particles did not give any electron diffraction pattern. The morphology of untreated carbon black and laser-processed carbon black samples is shown in Fig. 2. The specific surface areas of untreated carbon black, carbon black after laser treatment and the laser-processed carbon black samples after enrichment by 80% oxidation at 510°C were 32, 28.5, and 29 $m^2/gm$, respectively. Results of transmission electron microscopy indicated that the material after treatment was crystalline and contained graphite, chaoite, and diamond particles. No α or β carbynes or lonsdaleite particles were observed in the TEM study. Again, Fedoseev *et al.*[13] pointed out that the presence of lonsdaleite was not unambiguously established from their results.

A micrograph of a diamond particle and a convergent beam electron diffraction pattern from the particle are shown in Fig. 3. The diamond crystal possessed a streaked structure due to {111} twinning. The electron diffraction pattern shown in Fig. 3(b) possesses all the cubic diamond reflections along with the forbidden {002} and $\{2\bar{2}2\}$ reflections that are commonly observed in synthetic diamonds. The forbidden reflections are due to twinning and double diffraction. For example, the {002} spot was observed due to reflections from $\{1\bar{1}1\}$ and $\{\bar{1}\bar{1}1\}$ planes. The splitting in the spots in the pattern is also due to twinning and double diffraction. One of the spots stemming from the {111} twin structure is arrowed. Weak reflections from double diffraction are also seen in the pattern. The interplanar spacings computed from the diffraction pattern are presented in Table 2. The computed values are in good agreement with the corresponding values for diamond listed in the powder diffraction file. The lattice parameter computed from the electron diffraction data is 3.62 Å which agrees, within experimental errors, with the value 3.54 Å reported in the literature.

The inplanar spacings computed from the selected area electron diffraction pattern of chaoite particles

Table 1. Laser–carbon processing experiments

| No. | Material | Size (μm) | Purity (%) | Atmos. | Feed Rate (mg/s) | Laser Mode | Power Density ($W/cm^2$) | No. of Passes |
|---|---|---|---|---|---|---|---|---|
| 1 | Graphite | 43 | >97.5 | air | — | cw | $1 \times 10^6$ | 10 |
| 2 | Graphite | 43 | >97.5 | air | 4.0 | cw | 4250 | 5 |
| 3 | Graphite | 43 | >97.5 | air | 4.0 | pulsed* | 330000 | 5 |
| 4 | Graphite | 1 | >99.9995 | air | 5.0 | cw | $1 \times 10^6$ | 5 |
| 5 | Graphite | 1 | >99.9995 | air | 4.0 | pulsed* | 330,000 | 5 |
| 6 | Graphite | 1 | >99.9995 | argon | 5.0 | cw | 217,000 | 5 |
| 7 | Graphite | 1 | >99.9995 | argon | 5.0 | cw | 177,000 | 5 |
| 8 | Carbon Black | 0.043 | >99.0 | air | 4.0 | cw | 4200 | 7 |
| 9 | Carbon Black | 0.043 | >99.0 | air | 4.0 | pulsed* | 330,000 | 7 |
| 10 | Carbon Black | 0.043 | >99.0 | air | 4.0 | pulsed** | 7,640 | 5 |

*2 ms pulse width, 100 Hz.
**Nd-YAG laser, 2.2 ms pulse width, 190 Hz.

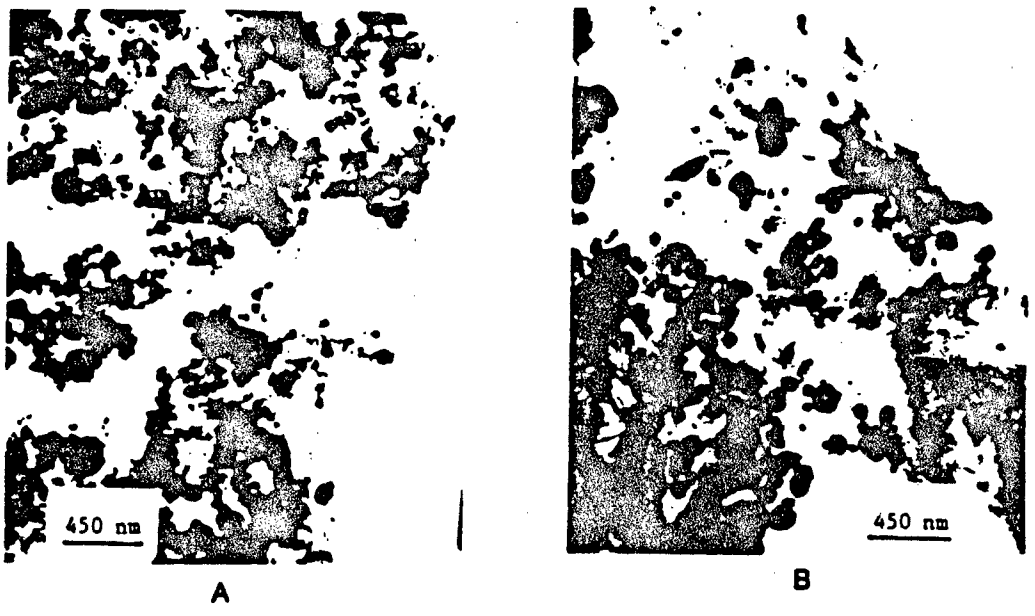


Fig. 2. Transmission electron micrographs of (A) unprocessed and (B) laser-processed carbon black sample. (See Table 1, Sample No. 9 for experimental conditions.)

are presented in Table 2, together with the corresponding data from the powder diffraction file. It is observed that the computed values agree, within the range of experimental errors, with the available interplanar spacing data. The lattice parameters $a_o$ and $c_o$ computed from the data were 8.86 and 14.14, respectively. These values agree well with the $a_o$ = 8.95 Å and $c_o$ = 14.08 Å values reported by Goresy and Donnay[16]. The electron diffraction study also indicated the presence of graphite in the enriched sample. Under the microscope, the high pressure phases were observed more frequently in the pulsed laser processed sample as compared to the sample processed in the continuous wave mode.

Results of x-ray diffraction studies indicated the presence of diamond, chaoite, and graphite. No α or β carbynes were detected. The x-ray diffraction data of untreated carbon black and laser-treated carbon black samples are presented in Table 3. In samples treated with both continuous wave (sample 8) and pulsed (sample 9) laser irradiations, major peaks of diamond were present. All reflections of cubic diamond were observed in the samples treated in the pulsed mode. Although it can be argued that several of the interplanar spacings listed in Table 2 are common to both cubic diamond and lonsdaleite, the interplanar spacing at 0.89 Å observed in sample 9 is unique to cubic diamond. Furthermore, lonsdaleite particles were not detected in the TEM work.

In the electron diffraction work, it was observed that the frequency of occurrence of chaoite particles in the sample was rather low. This observation is in agreement with the x-ray data where only a few chaoite reflections are observed. However, the *d*-spacings of 2.49 Å for sample 8 and 1.38 Å for sample 9 correspond exclusively to chaoite and to no other carbon form. In the diffraction pattern for the carbon black samples, the *d*-spacings at 3.35 and 3.34 Å correspond to the 100 intensity peak of rhombohedral graphite and cannot be attributed to any other carbon form, that is, diamond, lonsdaleite, chaoite, α and β carbynes. The 100 intensity line of hexagonal graphite lies at 3.36 Å which is fairly close to the strong 3.35 Å and 3.34 Å lines observed in the patterns. Thus, some carbon black was indeed graphitized. Fedoseev *et al.* indicated that some particles gave electron diffraction patterns in accordance with reflections for both hexagonal and rhombohedral graphite. It is to be noted that the carbon black sample contained more than 99% carbon and the *d*-spacing values at 4.13 Å, 3.73 Å, and 1.99 Å in samples 8 and 9 are attributed to the presence of impurities since these lines were also present in the starting carbon black sample.

From the x-ray data, it is observed that chaoite, diamond, and graphite were present in the processed material. The presence of lonsdaleite could not be unambiguously established. It has been proposed that the transformation to diamond from carbon black takes place after graphitization[17]. Indeed, Fedoseev *et al.*[12] achieved better transformation to diamond when polycrystalline graphite was used as the starting material as compared to carbon black. However, no high-pressure phases were detected in the laser-processed graphite samples in our experiments. This apparent discrepancy must be viewed in the context of the findings of DeCarli and Jamieson[5] who indicated that only the rhombohedral form of

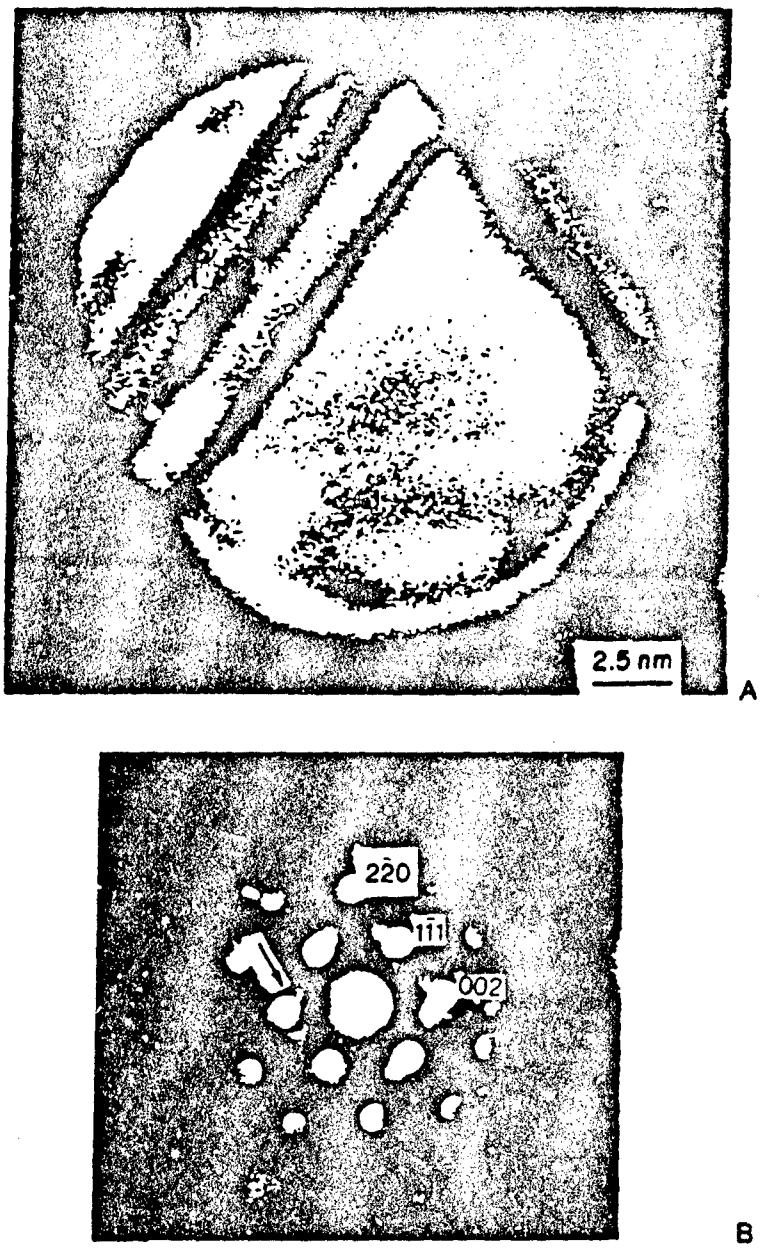


Fig. 3. (A) Transmission electron micrograph of a particle giving diamond pattern and (B) electron diffraction pattern of diamond from the particle shown above.

Table 2. Interplanar spacings of diamond and chaoite

| hkl | $d$(Å) (calculated) | $d$(Å) (powder diffraction file) |
|---|---|---|
| Diamond | | |
| 111 | 2.09 | 2.06 |
| 220 | 1.28 | 1.26 |
| 311 | 1.09 | 1.08 |
| 400 | 0.91 | 0.89 |
| 331 | 0.83 | 0.82 |
| $a_o$ | 3.62 | 3.57 |
| Chaoite | | |
| 110 | 4.63 | 4.47 |
| 301 | 2.63 | 2.55 |
| 304 | 2.11 | 2.10 |
| 401 | 1.87 | 1.81 |
| 227 | 1.54 | 1.50 |
| 600,506 | 1.31 | 1.29 |
| $a_o$ | 8.86 | 8.95 |
| $c_o$ | 14.1 | 14.08 |

graphite could be transformed to diamond by application of high dynamic pressure. In their experiments, no transformation occurred in the hexagonal form of graphite. Although Fedoseev *et al.*[12,13] did not report the crystal structure of graphite used in their experiments, in view of the results of DeCarli and Jamieson[5] it appears that the graphite used by Fedoseev *et al.*[12,13] probably contained some rhombohedral form.

The mechanism for transformation is not known. Fedoseev *et al.* speculated that the transformation of carbon black to diamond occurs because of rapid heating and cooling. When particles of sufficiently small size are exposed to the laser beam, their temperatures rise so rapidly that the equilibrium thermal expansion cannot occur. As a result, the particles experience a very large stress at high temperature which results in the phase transformation. The high cooling rate is important to ensure preservation of the transformed product phases. In our experiments, beam pulsing led to somewhat higher yields, which is consistent with both rapid heating due to higher power density (Table 1) and rapid cooling when the beam is switched off during pulsing. When we used a Nd-YAG laser of 1.06 μm wavelength, the yield of the material was insignificant.

The Derjaguin laser method of synthesis of high-pressure phases discussed in this article is not limited to the carbon system. Fedoseev *et al.* synthesized the high pressure polymorphs of silica, namely coesite and stishovite, from α-quartz by the laser process. We found that α-quartz particles on interacting with the laser beam not only transform to coesite and stishovite but to two other high pressure polymorphs having $Fe_3N$ type and α-$PbO_2$ type crystal structure. Work is now in progress on several other systems.

## 4. SUMMARY AND CONCLUSIONS

The report of Fedoseev and Derjaguin that diamonds can be made by merely exposing carbon to a modest laser flux in air has been confirmed. Finely divided carbon black particles of 0.043 μm average size were transformed into diamond, chaoite, and graphite. The diamond crystals exhibited twinning and {002} and {222} forbidden reflections commonly observed in synthetic diamonds. The extent of conversion was somewhat higher when the processing was carried out in the pulsed mode at a high laser power density.

Table 3. X-ray diffraction data for unprocessed and laser-processed carbon black samples

| Untreated Carbon Black | | Laser-treated 8 | | Carbon Black 9 | | |
|---|---|---|---|---|---|---|
| $d$(Å) | $I/I_o$ | $d$(Å) | $I/I_o$ | $d$(Å) | $I/I_o$ | Peak Pertaining to the Carbon Phase |
| 4.14 | vs | 4.13 | vs | 4.13 | vs | |
| 3.72 | s | 3.73 | vs | 3.73 | vs | |
| — | — | 3.35 | s | 3.34 | vs | Graphite (3.35, 100) |
| — | — | 2.82 | w | — | — | — |
| — | — | 2.49 | vw | — | — | Chaoite (2.46, 40) |
| — | — | 2.14 | vw | — | — | Graphite (2.13, 10); Chaoite (2.10, 40) |
| — | — | 2.06 | w | 2.06 | s | Diamond (2.06, 100); Lonsdaleite (2.06, 100) |
| 1.99 | s | 1.98 | w | 1.99 | w | |
| — | — | — | — | 1.82 | w | Graphite (1.82, 5) |
| — | — | — | — | 1.38 | vw | Chaoite (1.37, 20) |
| — | — | — | — | 1.26 | w | Diamond (1.26, 25); Lonsdaleite (1.26, 75) |
| | | | | 1.07 | w | Diamond (1.08, 16); Lonsdaleite (1.08, 50); Chaoite (1.08, 20) |
| — | — | — | — | 0.89 | w | Diamond (0.89, 8) |
| — | — | — | — | 0.82 | w | Diamond (0.82, 16); Lonsdaleite (0.82, 25) |

vs = very strong; s = strong; w = weak; vw = very weak.

CuKα radiation at 40 kV and 16 mA was used with nickel filter. Exposure times were 24 h for untreated carbon black and 72 h and 96 h for samples 8 and 9, respectively.

*Acknowledgment*—Financial support for this work was provided by the Office of Naval Research. We are grateful to Prof. K. Mukherjee and Dr. P. A. A. Kahn for their help in using the Nd-YAG laser facility at the Michigan State University.

## REFERENCES

1. F. P. Bundy, H. T. Hall, H. M. Strong, and R. H. Wentorf, Jr., *Nature* **176**, 51–55 (1955).
2. H. Liander and E. Lundblad. *Arkiv. Kemi* **16**, 139–149 (1960).
3. F. P. Bundy, *J. Chem. Phys.* **38**, 631–663 (1963).
4. L. F. Vereshchagin, Ya. A. Kalashnikov, E. M. Feklichev, I. V. Nikol'skaya, and L. M. Tikhomirova, *Sov. Phys. Doklady* **10**, 534–537 (1965).
5. P. S. DeCarli and J. C. Jamieson, *Science* **133**, 1821–1822 (1961).
6. G. K. Cowan, B. W. Dunnington, and A. H. Holtzman, U.S. Patent 3,401,019 / E.I. duPont de Nemours and Co. (1966).
7. B. V. Derjaguin and D. V. Fedoseev, *Scientific American* **233**(5), 102–109 (1975).
8. B. V. Derjaguin and D. v. Fedoseev, *Growth of Diamond and Graphite from the Gas Phase*, Izd. Nauka, Moscow (1977).
9. B. V. Spitsyn, L. L. Bouilov, and B. V. Derjaguin, *J. Cryst. Growth* **52**, 219–226 (1981).
10. S. Matsumoto, Y. Sato, and M. Tsutsumi. *J. Mat. Sci.* **17**, 3106–3112 (1982).
11. R. Messier, A. R. Badzian, T. Badzian, K. E. Spear, P. Bachmann, and R. Roy, *Thin Solid Films* **153**, 1–9 (1987).
12. D. V. Fedoseev, V. L. Bukhovets, I. G. Varshavskaya, A. V. Lavrent'ev, and B. V. Derjaguin, *Carbon* **21**, 237–241 (1983).
13. D. V. Fedoseev, I. G. Varshavskaya, A. V. Lavrent'ev, and B. V. Derjaguin, *Powder Technology* **44**, 125–129 (1985).
14. M. Alam, T. DebRoy, R. Roy, and E. Breval, *Applied Physics Letters*, Vol. **53**, 1687–1689 (1988).
15. M. Alam, T. DebRoy, and R. Roy, *Carbon* **26**, 591–593 (1988).
16. A. El Goresy and G. Donnay, *Science* **161**, 363–365 (1968).
17. G. N. Bezrukov, V. P. Gutuzov, and M. I. Samoilovich, *Synthetic Diamond*, Nerda Publishers, Moscow (1976).

# High-pressure phases of $SiO_2$ made in air by Fedoseev–Derjaguin laser process

M. Alam, T. DebRoy,[a] R. Roy,[b] and E. Breval
*Materials Research Laboratory, Pennsylvania State University, University Park, Pennsylvania 16802*

(Received 5 July 1988; accepted for publication 23 August 1988)

Exposure of a falling stream of 1 $\mu$m average size $\alpha$-quartz particles to a continuous wave or pulsed $CO_2$ laser beam in air resulted in the formation of a complete series of high-pressure phases of silica: coesite, stishovite, and apparently even denser forms with $\alpha$-$PbO_2$ and $Fe_2N$ structures. Since the laser exposure technique works with the carbon black to diamond transition, the technique is confirmed as a simple and generally applicable means to achieve the same effects as exposure to several hundred kilobars pressure.

For the last several decades, synthetic hard materials have been produced by the application of high static and dynamic pressures at elevated temperatures. Familiar examples include synthesis of diamond[1–4] and the production of high-pressure phases of the oxides of group IV elements, particularly silica.[5–13] All these techniques for synthesis involved application of very high pressures, often of the order of several tens of thousands of atmosphere at elevated temperatures where the targeted high-pressure phase is thermodynamically stable.

In 1983 Fedoseev *et al.*[14] reported a radically different and incredibly simple method of diamond synthesis. The technique involved exposing a flowing loose powder of carbon black and graphite, in air, to a modest laser flux. They claimed that this simple treatment resulted in the transformation of fine carbon black and graphite particles to chaoite, lonsdaleite, and diamond. In a subsequent article in 1985, Fedoseev *et al.*[15] reviewed their diamond work and indicated that the technique could also be applied to the synthesis of high-pressure phases of silica and boron nitride. Fedoseev *et al.* synthesized two high-pressure polymorphs of silica, namely, coesite and stishovite, from $\alpha$-quartz by the laser process. Their work opened up a potentially new technique for the synthesis of high-pressure phases.

We have verified the diamond work[16] by exposing fine particles of carbon black to continuous wave and pulsed laser radiation in air at various power densities. X-ray and electron diffraction of the enriched laser-processed samples indicated the formation of cubic diamond, chaoite, and both hexagonal and rhombohedral graphite. The diamond was observed as ~10 nm twinned crystals.

The objective of the work reported here was to confirm and extend the findings of Fedoseev *et al.* with regard to silica. We have not only produced coesite and stishovite by this technique, as reported by Fedoseev *et al.*, but also two other silica phases having $\alpha$-$PbO_2$ and $Fe_2N$ structures. These phases are the highest pressure phases of silica ever made by this or any other technique.

Fine particles of $\alpha$-quartz were exposed to both continuous wave and pulsed $CO_2$ laser beams at various power densities. The processed material was concentrated with respect to the product phases and analyzed by x-ray and electron diffraction for the identification of the products. A schematic diagram of the experimental setup is shown in Fig. 1. The setup consisted of an Everlase model 525 $CO_2$ laser and an electrically powered vibrating feeder. The particles were injected horizontally and were treated with a vertically transmitted laser beam. The laser-processed particles were collected in a glass beaker. The type of material used and the specific conditions of the experiments are presented in Table I. Examination of Table I indicates that in general transformation occurred when pulsed laser radiation was used. For samples 7, 8, and 9 the pulse lengths used were 3, 3, and 2 ms, respectively, while the frequency of pulsing was 100, 400, and 100 Hz, respectively.

After laser processing, the powder was dispersed in a hydrofluoric acid solution. The undissolved portion was cleaned, dried, and characterized. The yield of the high-pressure phases in all the experiments was very small ( $< 0.5\%$ ) and in all cases melting of some silica particles was observed.

The $\alpha$-quartz particles on exposure to either continuous wave or pulsed $CO_2$ laser beam were transformed to high-pressure polymorphs of silica, namely, coesite, stishovite, $\alpha$-$PbO_2$-type, and $Fe_2N$-type modifications.

Two selected area electron diffraction patterns obtained by tilting a coesite grain to different degrees are shown in Figs. 2(a) and 2(b). The *d*-spacing values calculated from the diffraction patterns are presented in Table II. The diffraction pattern shown in Fig. 2(b) contains a dense row, caused by a long *b* axis. Since among the various silica phases only coesite and tridymite have a long *b* axis and x-ray dif-

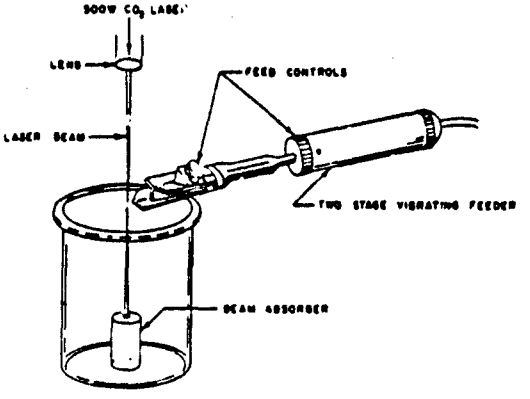


FIG. 1. Schematic diagram of the experimental setup.

[a] Also affiliated with the Department of Materials Science and Engineering.
[b] Also affiliated with the Department of Geosciences.

 0003-6951/88/441687-03$01.00  

TABLE I. Experimental conditions for processing. Material: $\alpha$-quartz; average particle size: 1 $\mu$m; purity: 99.99%; atmosphere: air

| Feed rate (mg/s) | Laser mode | Power density (kW/cm$^2$) | No. of passes | Transformation observed |
|---|---|---|---|---|
| 15 | continuous wave | 0.5 | 6 | no |
| 15 | continuous wave | 1.6 | 6 | no |
| 15 | continuous wave | 4.2 | 6 | yes |
| 4 | continuous wave | 10.0 | 10 | no |
| 5 | continuous wave | 17.8 | 10 | no |
| 4 | continuous wave | 1200.0 | 10 | yes |
| 4 | pulse | 330.0 | 7 | yes |
| 4 | pulse | 1000.0 | 10 | yes |
| 4 | pulse | 900.0 | 2 | yes |

TABLE II. Interplanar spacings of coesite and stishovite.

| *hkl* | *d*(Å) (calculated) | *d*(Å) (powder diffraction file) |
|---|---|---|
| Coesite | | |
| 131, 132 | 2.63 | 2.69 |
| 241, 201 | 2.42 | 2.33 |
| 221, 240 | 2.14 | 2.18 |
| 330, 033 | 1.86 | 1.84 |
| · · · | 1.64 | 1.66 |
| · · · | 1.53 | 1.55 |
| · · · | 1.34 | 1.35 |
| · · · | 1.32 | 1.32 |
| Stishovite | | |
| 110 | 2.92 | 2.96 |
| 200 | 2.06 | 2.09 |
| 220 | 1.46 | 1.48 |
| 310 | 1.30 | 1.32 |

fraction data do not indicate the presence of tridymite, the dense row is an indication of the presence of coesite. The distance between the spots in the dense row is about 12 Å which is equal to the distance between {010} planes of coesite. The {010} reflection is forbidden in monoclinic structure (coesite), but can become visible due to double diffraction. A particle containing a dense row was isolated. A dark-field micrograph of such a particle is shown in Fig. 3(a). A selected area electron diffraction pattern from the particle in Fig. 3(a) is presented in Fig. 3(b). The pattern clearly indicates the dense row spots corresponding to {010} planes.

Stishovite grains were found in small groups in the specimen. A dark-field micrograph of a typical group of stishovite grains is shown in Fig. 4(a). A selected area diffraction (SAD) pattern from the particles in Fig. 4(a) is presented in Fig. 4(b). Only the {*hk*0} reflections of stishovite can be observed in the diffraction pattern. The *d*-spacing values calculated from the diffraction patterns are presented in Table II. Several electron diffraction patterns were taken by tilting the specimen. However, no significant change in the patterns was observed due to the very small size of the particles. The presence of only the {*hk*0} reflections in the diffraction pattern indicates preferred orientation of the stishovite grains which lie on their {001} planes. It seems that several stishovite grains lie on top of each other in the same way as clay minerals and other layered minerals do. When hit by the electron beam, these grains are charged and split away from each other in the {001} plane. On splitting, the stishovite grains lie on the {001} planes and have approximately the same orientation in the {001} plane within about 15°. This is why only the {*hk*0} reflections are observed. The presence of an incomplete ring pattern indicates that the pa ticles are neither completely randomized nor have the san crystallographic orientation when lying on the {001} plane

The x-ray diffraction analysis of the laser-treated quartz samples indicated the presence of coesite, stishovi $Fe_2N$-type and $\alpha$-$PbO_2$-type silica along with $\alpha$ quartz. T x-ray diffraction data are presented in Table III. In this ble, the peaks corresponding only to $\alpha$-quartz are not p sented.

Examination of Table III indicates that in both the ser-processed samples several of the observed x-ray diffr tion peaks can be attributed to coesite. Some of the pe attributed to coesite are common to other silica forms. Ho ever, the x-ray diffraction peaks at 3.09, 2.69, 2.03, and 1 Å observed in the two samples (Table III) are unique coesite. Furthermore, the highest intensity peak of coesit 3.09 Å is present in both the laser-processed samples.

Several of the x-ray diffraction peaks observed in e sample can be attributed to stishovite (Table III). A several of these peaks are common to other phases of sil However, peaks at 2.959 and 1.215 Å in sample 7 are uni to stishovite (Table III). Furthermore, the peak at 2.9 is the highest intensity peak of stishovite. This peak is p ent in sample 7. The second and third major peaks of sti vite at 1.53 and 1.98 Å are also present in both the l processed silica samples.

Several peaks of the $\alpha$-$PbO_2$-type silica were observ each of the laser-processed samples. All the observed p are, however, common to other forms of silica excep peak at 2.35 Å observed in sample 7 which is uniq

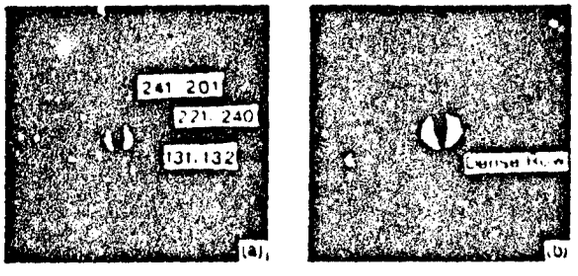


FIG. 2. Convergent beam electron diffraction patterns from a coesite particle.

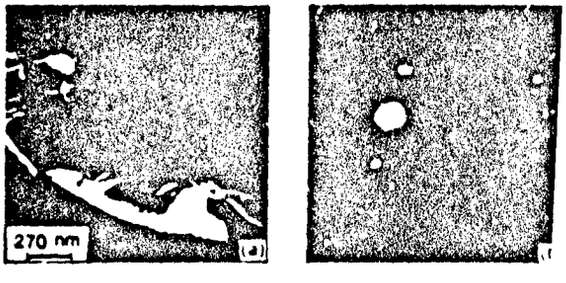


FIG. 3. (a) Dark-field micrograph of a particle containing a dense r Convergent beam electron diffraction pattern from particle in (a)

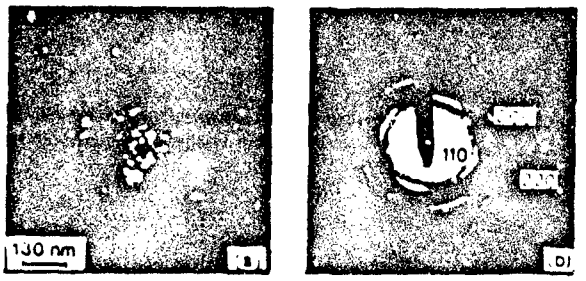


FIG 4. (a) Dark-field micrograph of stishovite grains. (b) Selected-area electron diffraction pattern from the particles in (a).

$\alpha$-$PbO_2$-type silica. In both the samples one of the two strong peaks of $\alpha$-$PbO_2$ at 2.08 Å is present. This peak, however, is common to other forms of silica. Furthermore, in both the samples at least one of the three moderately strong peaks of $\alpha$-$PbO_2$-type silica at 2.35, 2.25, and 2.15 Å is present. Again, except for the peak at 2.35 Å which is unique to $\alpha$-$PbO_2$ silica, the other peaks are common to other silica forms.

The x-ray diffraction data presented in Table III indicate that $Fe_2N$-type silica was present in the processed sample. Of the various peaks that can be attributed to $Fe_2N$-type silica, three peaks at 1.508, 1.952, and 1.186 Å are unique to $Fe_2N$-type silica (Table III). The other peaks are common to other forms of silica. The first three major peaks of $Fe_2N$-type silica in order of decreasing intensity occur at 1.508, 1.952, and 1.281 Å. At least one of these peaks occurs in each of the laser processed samples. It must be mentioned that Liu *et al.*[9] who first synthesized $Fe_2N$-type-silica using the diamond anvil cell detected only the first three major peaks of the new phase in the x-ray diffraction pattern. The presence of only one or two unique major peaks of $Fe_2N$-type silica in our samples is indicative of the presence of a very small amount of $Fe_2N$-type silica in the samples.

The presence of coesite, stishovite, $\alpha$-$PbO_2$, and $Fe_2N$-type signals in the x-ray diffraction pattern indicates that during processing, the particles were exposed to several hundred kilobars of pressure. Fedoseev *et al.*[14,15] speculated that the transformation to high-pressure phases occurs because of rapid heating and cooling. When particles of sufficiently small size are exposed to laser beam, their temperatures rise so rapidly that the equilibrium thermal expansion cannot occur. As a result, the particles experience very large stress at high temperature which results in phase transformation. The high cooling rate is important to ensure preservation of the transformed produce phases. In our experiments, beam pulsing led to somewhat higher yields which is consistent with both rapid heating due to higher power density (Table I) and rapid cooling when the beam is switched off during pulsing. However, the mechanism of transformation is not clearly known. If, indeed, the mere exposure to high fluxes of photons can cause *solid-state* transformations, the method becomes a general tool in materials science. Understanding the mechanism offers a challenge and an opportunity to extend its use as a tool for material synthesis which could possibly produce phases unattainable by other means. The implications for theories for cosmology and stellar and planetary formation could also be far reaching.

TABLE III. X-ray diffraction data of laser-processed $SiO_2$ samples. Phases A, B, C, D, and E indicate coesite, stishovite, $\alpha$ $PbO_2$-type, and $Fe_2N$-type silica, and $\alpha$ quartz, respectively.

| Interplanar ±6 | Spacing Å ±7 | Interplanar spacings and intensities of catalogued phases |
|---|---|---|
| 3.029 | 3.055 (S) | A (3.09, 100) |
| ... | 2.920 (S) | B (2.959, 100) |
| 2.685 | ... | A (2.69, 10) |
| 2.377 | ... | C (2.35, M) |
| ... | 2.334 (M) | A (2.33, 4), C (2.351, M) |
| 2.280 | 2.285 (VW) | A (2.29, 8), C (2.25, M), E (2.282, 12) |
| ... | 2.230 (M) | B (2.246, 18), C (2.25, M), E (2.237, 4) |
| 2.200 | ... | A (2.18,4), D (2.218, 12) |
| ... | ... | C (2.152, M), E (2.128, 9) |
| 2.085 | 2.072 (W) | B (2.09, 1), D (2.056,-), C (2.08, S) |
| ... | 2.025 (VW) | A (2.03, 6) |
| 1.978 | 1.988 (VW) | B (1.981,35), C (1.994), E (1.980, 6) |
| ... | 1.946 (W) | D (1.952, 90) |
| ... | 1.899 (VW) | A (1.84, 4), B (1.87, 14), C (1.875, VW) |
| 1.821 | ... | C (1.836, -), E (1.817, 17) |
| ... | 1.790 (M) | A (1.79, 8), E (1.801, < 1) |
| 1.693 | ... | A (1.70, 10) |
| 1.668 | ... | A (1.66, 2), E (1.659, 3) |
| 1.577 | 1.588 (VW) | A (1.58, 6), C (1.588, W) |
| 1.540 | 1.541 (VW) | A (1.545, 10), B (1.53, 50), C (1.555, W) E (1.5418, 9) |
| 1.523 | ... | D (1.508, 100) |
| ... | 1.474 (M) | B (1.478, 18), C (1.497, M) |
| ... | 1.419 (W) | A (1.418, 2), E (1.4189, < 1) |
| 1.404 | 1.401 (VW) | A (1.409, 4), E (1.418, < 1) |
| 1.375 | 1.374 (M) | D (1.371, extinct), E (1.3752, 7) |
| 1.334 | 1.323 (VW) | A (1.321, 2), B (1.333, 10) |
| 1.276 | 1.286 (VW) | A (1.285, 6), B (1.291, 2), C (1.297, -), D (1.281, 56) |
| 1.239 | 1.227 (W) | B (1.235, 25), C (1.232, VW), E (1.236, 4) D (1.223, extinct), E (1.2285, 1) |
| ... | 1.214 (VW) | B (1.215, 10) |
| 1.182 | 1.180 (W) | A (1.171, 6), B (1.185, 2) E (1.1838, 4), E (1.1804, 3) |
| ... | 1.166 (VW) | D (1.166, 15) |
| ... | 1.063 (W) | B (1.062, 2), E (1.0635, < 1) |
| 1.043 | 1.042 (VW) | B (1.045, 2), E (1.0437, 2) |

S = strong; M = moderate; W = weak; VW = very weak.

Financial support for this work was provided by the Office of Naval Research.

[1] F. P. Bundy, H. T. Hall, H. M. Strong, and R. H. Wentorf, Jr., Nature 176, 51 (1955).
[2] G. R. Cowan, B. W. Dunnington, and A. H. Holtzman, U.S. Patent No 3 401 019 to E. I. DuPont de Nemours and Co. (1966).
[3] P. S. Decarli and J. C. Jamieson, Science 133, 1821 (1961).
[4] F. P. Bundy, J. Chem. Phys. 38, 361 (1962).
[5] L. Liu, in *High Pressure Research in Geophysics*, edited by S. Akimoto and M. H. Manghnani (Kluwer, Boston, 1982), p. 349.
[6] L. Coes, Science 118, 131 (1953).
[7] S. M. Stishov and S. V. Popova, Geochemistry (USSR) 10, 923 (1961).
[8] F. Dachille and R. Roy, Zeit. Krist. 111, 451 (1959).
[9] L. Liu, W. A. Bassett, and J. Sharry, J. Geophys. Res. 83, 2301 (1978).
[10] J. Wackerle, J. Appl. Phys. 33, 922 (1962).
[11] R. F. Trunin, G. V. Simakov, M. A. Podurets, B. N. Moiseyev, and L. L. Popov, Izv. Acad Sci. USSR Phys. Solid Earth 1, 13 (1971).
[12] V. N. German, M. A. Podurets, and R. G. Trunin, Sov. Phys. JETP 37, 107 (1973).
[13] I. Jackson and T. J. Ahrens, Phys. Earth Planet. Inter. 20, 60 (1979).
[14] D. V. Fedoseev, V. L. Bukhovest, I. G. Varshavskaya, A. V. Lavrent'ev, and B. V. Derjaguin, Carbon 21, 237 (1983).
[15] D. V. Fedoseev, I. G. Varshavskaya, A. V. Lavrent'ev, and B. V. Derjaguin, Powder Technol. 44, 125 (1985).
[16] M. Alam, T. DebRoy, R. Roy, and E. Breval, Carbon (in press).

# TEM characterization of structural changes in graphite plates due to pulsed $CO_2$ laser irradiation

E. BREVAL, M. ALAM*, T. DEBROY, R. ROY
*The Pennsylvania State University, University Park, PA 16802, USA*

Exposure of a solid to very high photon fluxes can generate high temperatures and pressures in some combinations. The above mentioned fact is indeed the basis of laser fusion research. In the first half of this decade Fedoseev, Derjaguin and co-workers at the Institute of Physical Chemistry in Moscow discovered an extraordinary phenomenon. They demonstrated that many significant high pressure phases including diamond [1, 2], stishovite ($SiO_2$) [2] and cubic BN [2] can be made by exposing fine particles of carbon black, α-quartz and h-BN, respectively, to modest $CO_2$ laser fluxes in air. These results have been reproduced and extended by a Penn State research group [3–5]. In all cases, the yield of the transformed product was rather low, although lower pulse length and higher energy/pulse improved the yield to some extent.

In all the work carried out so far, TEM was used in addition to X-ray diffraction to identify the product phases, which had to be concentrated by special procedures [3–5]. Such procedures are very tedious because the product appears only in small quantities of nanometre size particles in a large amount of untransformed material. To overcome this difficulty, it was decided to perform the irradiation on 'large' bulk samples and to examine the irradiated area by TEM. We irradiated thin graphite discs with a pulsed $CO_2$ laser beam and characterized the material in the interior and along the laser induced crater wall. The purpose of this paper is to examine the nano- and micrometer structure of the region in and around the crater wall produced by the laser pulse(s).

High purity polycrystalline graphite discs (> 99.999% C, grain size ~ 1 to 10 μm, disc diameter = 25.4 mm, thickness = 10 mm) were irradiated with laser pulses under vacuum (pressure < 5 μm Hg) using an Everlase Model 525 $CO_2$ laser manufactured by Coherent Inc. The spots were produced by 1 ms duration pulses having a peak energy of 0.7 J. The frequency was 100 Hz and the total irradiation time was 1 sec. The size of the spots was 0.25 mm. The specimens for the TEM study were prepared by two methods. In the first case, material was carefully removed from the interior of the crater (base and side walls) and crushed lightly in a few drops of isopropanol. The slurry was then transferred to a carbon coated copper grid, dried and applied with a light carbon coating. In the second case, the crater was filled with a thick paste of graphite powder in a two component epoxy. After hardening the specimen was cut to a disc ~ 3 mm in diameter and then polished down to 0.05 μm alumina slurry on one side and dimpled from the other side down to 0.05 μm alumina slurry. The specimen was then ion beam thinned (gun voltage = 3 to 4 kV, gun current = 0.2 to 0.7 μA, specimen current ~ 3 μA) and applied with a light carbon coating. An ISI-DS 130 scanning electron microscope (SEM) was used together with an EM 420 transmission electron microscope (TEM) with the acceleration voltage of 120 kV. Either bright field (BF) or dark field (DF) images were obtained together with either selected area electron diffraction patterns (SAED) or convergent beam electron diffraction patterns (CBED).

In the specimen prepared by the first method, most of the material consisted or irregular grains of graphite. In this specimen, extremely small amounts of fine grained loose particles could be observed. A DF TEM

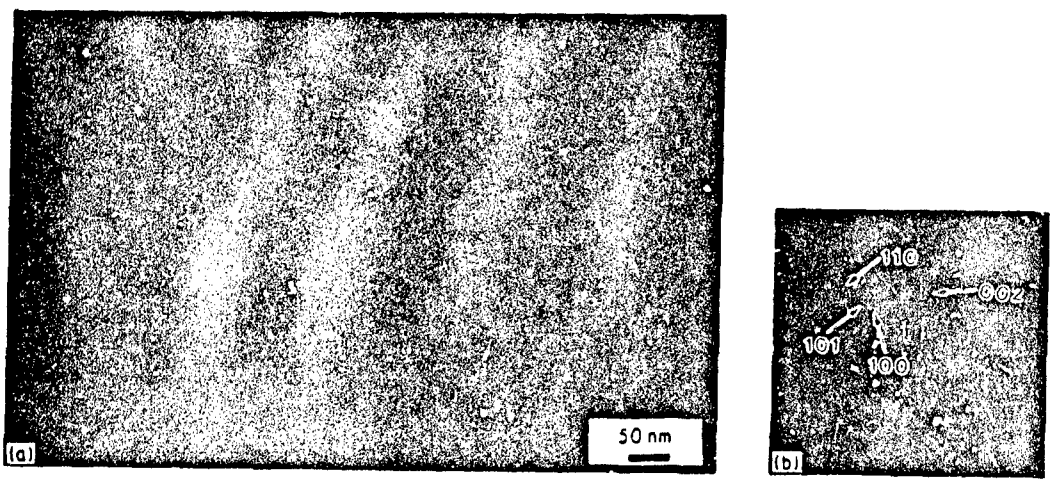


*Figure 1* (a) TEM DF image of material from the interior of the crater. (b) SAEDP from the loose fine grains shown in (a).

* Now with the New Mexico Institute of Mining and Technology, Socorro, NM 87801, USA.

0261-8028/90 $03.00 + .12 

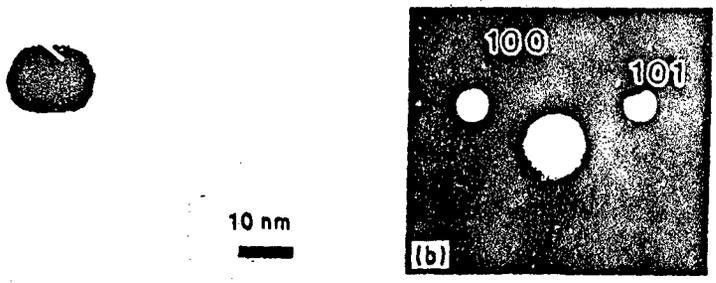


*Figure 2* (a) TEM BF image of one of the larger particles shown in Fig. 1a, exhibiting epitaxial growth of lonsdaleite with graphite. (b) C
pattern from particle shown in Fig. 2a, exhibiting 1 0 0 and 1 0 1 lonsdaleite reflections.

micrograph showing such particles is presented in Fig. 1a. These particles give a weak SAED ring pattern as shown in Fig. 1b. One diffuse ring at ~0.21 to 0.22 nm is clearly seen indicating that the particles could be lonsdaleite (the high pressure carbon polymorph with hexagonal structure). The reflections from 1 0 1 and 1 1 0 are barely visible at 0.192 and 0.126 nm, respectively. The 1 0 0 and 0 0 2 reflections correspond to *d*-spacing values of 0.219 and 0.206 nm, respectively. Hence the faint ring diffraction pattern is interpreted as stemming from lonsdaleite. A BF TEM micrograph of one such particle which is relatively large is presented in Fig. 2a along with an orientated CBED pattern (Fig. 2b) where the 1 0 0 and 1 0 1 reflections of lonsdaleite are clearly visible. On the BF image (Fig. 2a) differently contrasted parts of the grain parted by planes perpendular to ⟨1 0 0⟩ can be seen. This feature can be explained as an epitaxial growth of ⟨1 0 0⟩ lonsdaleite parallel to graphite as suggested by Bundy and Kasper [16]. They found that fine grained lonsdaleite was often 'epitaxially twinned' with graphite having the following planar symmetry: lonsdaleite (1 0 0) ∥ graphite (0 0 1). Although there was no three dimensional symmetry, since half of the atoms in the basal graphite plane must be displaced to fit into the (1 0 0) lonsdaleite structure, there w a two dimensional fit. Bundy and Kasper also fou the following directional symmetry: lonsdal [0 0 1] ∥ graphite [2 0 1] and lonsdaleite [0 1 0] ∥ grap [0 1 0] the latter of which could fit in our case (equ alent to overlapping of the lonsdaleite 1 0 0 reflex w the graphite 1 0 0 reflex). Since only the largest crys possessed such 'epitaxial twins' it was not possibl find any graphite reflections on the ring pattern Fig. 1b.

A scanning electron micrograph of the ion b thinned specimen is shown in Fig. 3. The crate clearly visible. Arrows indicate regions which w analyzed by TEM. Both BF and DF TEM imagin the crater wall are presented in Figs. 4a and respectively. The micrographs show the presenc almost equidimensional nanometre size grains in wall. The corresponding SAED pattern from region shown by the arrow in Fig. 4a is presente Fig. 4c. This pattern is very characteristic of the material and is interpreted as graphite. The pat indicates almost random orientation with a tend to more intense diffraction of the 0 0 2 and reflections in the direction arrowed on the BF in This more intense diffraction of a part of the 0 reflections in the direction perpendicular to the c wall shows that the grains have a tendency of ⟨0 being perpendicular to the crater wall. A scan electron micrograph of the same region of the w presented in Fig. 5. The arrow points to the r where the TEM images were obtained (Fig. 4) micrograph shows that the specimen near the c wall is rather thick indicating that the specimen the hole is more resistant to the ion beam thi compared to the graphite material used to fill t crater and the graphite disc. This is evident perusal of Fig. 4 where the width of the cl transparent area of the crater wall is only 1 300 nm as compared to 2 to 10 μm in undist graphite material. A DF TEM micrograph of a part of the crater wall is shown in Fig. 6a. The graph shows a small part of a graphite flake usec the crater (marked g). The figure clearly sho almost equidimensional nm size particles alo

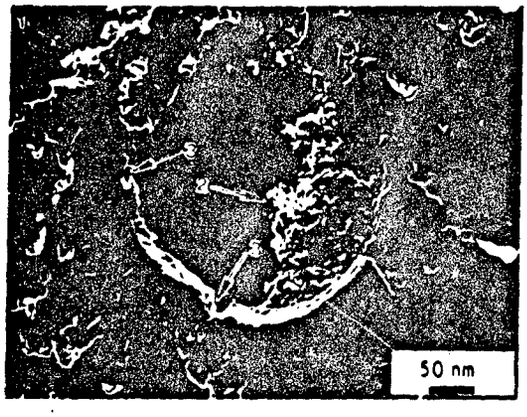


*Figure 3* SEM of ion beam thinned specimen. The arrows indicate regions of TEM investigations of the graphite plate (1), graphite powder inside the crater (2), and the crater wall (3).

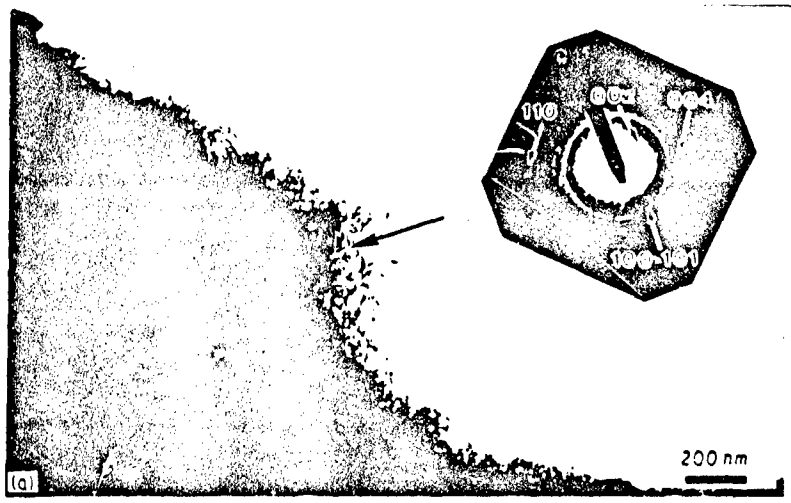


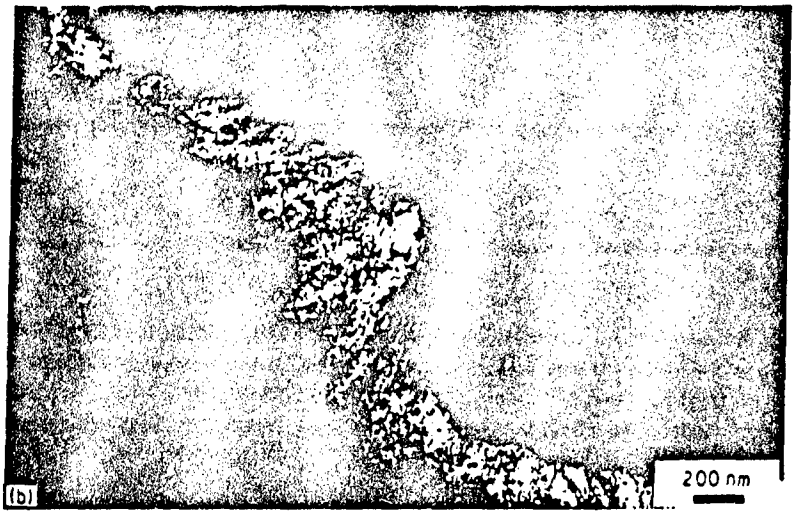


thinned specimen containing one nanometre size material (a) BF and (b) DF, both imaging the same region (c) corresponding SAED pattern showing more intense diffraction of 002 and 004 reflections in the direction arrowed on the BF image.

wall. The SAED pattern from the fine nanometre size particles is presented in Fig. 6b and represents only the fine particles and not graphite material from the graphite used to fill the crater or the graphite material in the graphite disc. Fig. 6b shows a complete ring pattern of graphite, but more intense reflections of the basal planes in the direction perpendicular to the crater wall show that the fine grained graphite particles have a tendency to be oriented with ⟨0001⟩ perpendicular to the crater wall. In order to study the local orientation effect, a CBED pattern was also made with a probe size of 40 nm covering several nanometre size grains (Fig. 6c). Again this is a complete pattern of graphite with a tendency of ⟨0001⟩ to be perpendicular to the crater wall.

In the ion beam thinned specimen, no lonsdaleite grains were observed, probably because they were lost before fixing with the epoxy or during the ion beam thinning.

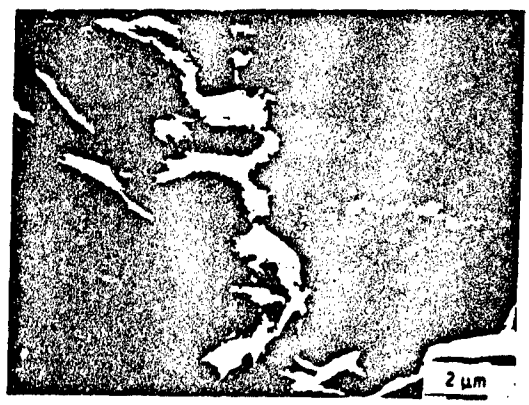


*Figure 5* SEM of a narrow region along the crater wall in the ion beam thinned specimen. The arrow indicates the region from which the TEM micrographs in Fig. 4 were obtained.

## Acknowledgements

The funding for this research was provided by the Office of Naval Research and by the Hoechst Celanese Corporation.

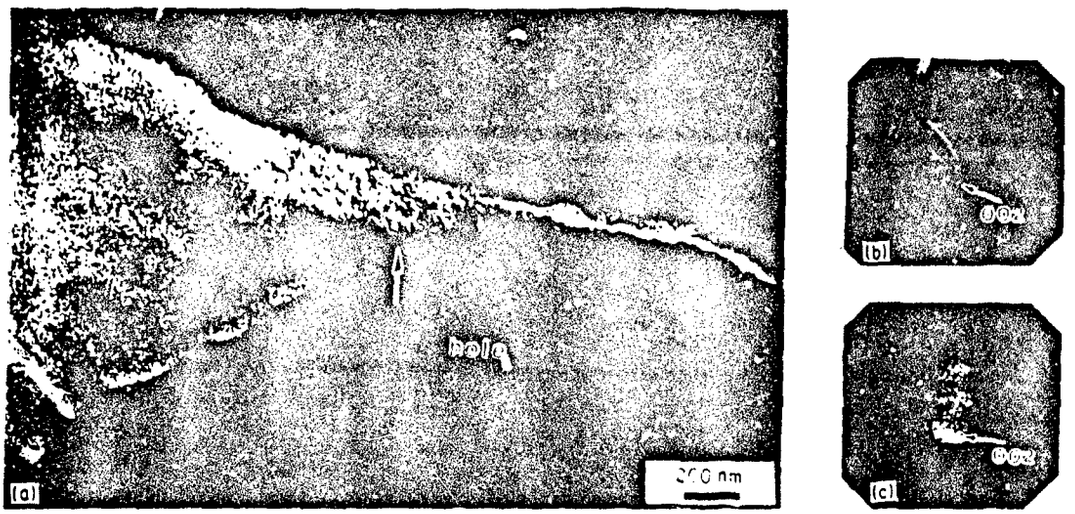


*Figure 6* (a) TEM of crater wall in the ion beam thinned specimen showing a little of the graphite inside the crater (marked g). The nanometre size particles in the crater wall are clearly visible (b) SAED and (c) CBED patterns of these particles showing more intense 09*l* reflections perpendicular to the crater wall.

## References


1. D. V. FEDOSEEV, V. I. BUKHOVETS, I. G. VARSHAVSKAYA, A. V. LAVRENT'EV and B. V. DERJAGUIN, *Carbon* **21** (1983) 237.
2. D. V. FEDOSEEV, I. G. VARSHAVSKAYA, A. V. LAVRENT'EV and B. V. DERJAGUIN, *Powder Technology* **44** (1985) 125.
3. M. ALAM, T. DEBROY, R. ROY and E. BREVAL, *Appl. Phys. Lett.* **53** (1988) 1687.
4. *Idem*, *Carbon* **27** (20) (1989) 289.
5. M. ALAM, T. DEBROY and R. ROY, *J. Amer. Ceram. Soc.* In press.
6. F. P. BUNDY and J. S. KASPER, *J. Chem. Phys.* **46** (1967) 3437.



*Received 2 January*
*and accepted 5 February 1990*

Carbon, 1988, vol 26, no 4



## Separation of synthetic diamond from carbon black by oxidation

*(Received 21 December 1987; accepted in revised form 17 February 1988)*

**Key Words** - Oxidation, carbon black, diamond

Traditionally, synthetic diamonds have been produced by subjecting carbon to high pressures and temperatures under which diamond is the thermodynamically stable form [1]. A few years ago, Fedoseev et al [2,3] reported a radically different and incredibly simple method of diamond synthesis. The technique involved exposing a flowing loose powder of carbon black and graphite, in air, to a modest laser flux to achieve the desired transformation. We have recently confirmed and extended [4,5] the findings of Fedoseev et al as a part of a larger program to produce a new class of synthetic hard materials. Since only partial conversion to diamond from carbon black is achieved in this process, it was necessary to separate diamond. Enrichment of diamond by selective dissolution of the low density carbon forms in nitric acid - sulfuric acid solution [6] was found to be unacceptably slow for our samples, perhaps because of the presence of significant amount of carbon black. Similarly, the gravity separation technique using a liquid of appropriate density [7] led to ineffective separation due to very small size of the solid particles. Due to these difficulties, the possibility of achieving effective separation by selective oxidation of laser treated solid mixture in both pure oxygen and carbon dioxide was explored.

The rates of oxidation of industrial grade diamond and carbon black powders, both containing less than 0.2% impurity, were studied by thermogravimetry using a Cahn microbalance. The oxidation rates of high purity graphite powder containing less than 2 ppm impurity were also measured for comparison. The average particle size of diamond, graphite and carbon black were 49 μm, 1μm and 0.043 μm respectively. Since the kinetics of oxidation of various carbon forms in carbon-dioxide is slow at temperatures below 1073 K, all experiments in $CO_2$ were carried out at 1273 K. These oxidation rates were compared with the corresponding rates in oxygen.

The results of the experiments are presented in Figure 1 as percentages of the initial weight lost vs. reaction time plots. The reproducibility of the rate data was tested by repeating oxidation tests for both graphite and diamond in oxygen. The times required for complete oxidation were 550 and 600 sec for the two experiments with graphite, and 870 and 960 sec for the experiments with diamond. The data in figure 1 indicate that under identical conditions all forms of carbon react at a higher rate in oxygen than in $CO_2$. Furthermore, it is also observed that diamond reacts at a faster rate as compared to graphite or carbon black in carbon dioxide. However, in oxygen, both graphite and carbon black react much faster than diamond. This apparent anomaly can be attributed, at least in part, to the differences in the surface areas of these materials. The approximate surface areas of all the three carbon forms were calculated as a function of the extent of oxidation on the basis of the shrinking core reaction model [8]. The reduction in the size of particles during oxidation was

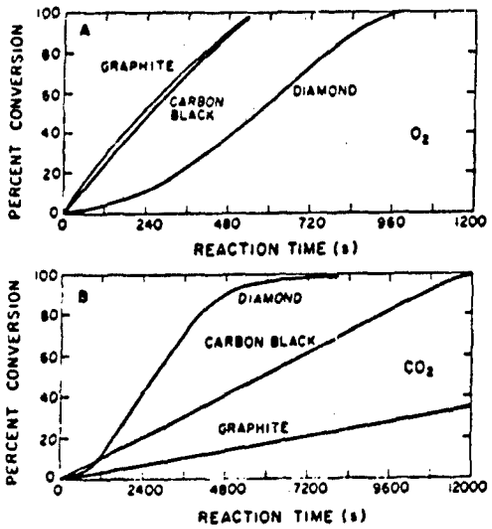


Fig. 1 Percent conversion vs reaction time. Reaction Temperature: 1273 K, Gas Flow Rate: 16.7 cc/sec, and Initial Sample Weight: 105 mg.

calculated utilizing the following equation:

$$r = r_o(1-F)^{1/3} \qquad (1)$$

where r and $r_o$ are the instantaneous and the initial radius of the particles and F is the extent of reaction defined as the ratio of the weight loss at a given time to the initial sample weight. The instantaneous oxidation rates, expressed in grams per second, were determined from the slope of the plots in figure 1 and the corresponding initial sample weights. The reaction rates per unit surface area, in gms/cm$^2$ sec, were then readily obtained from the surface area computed from the following relation:

$$s = 3W_o r^2/r_o{}^3\rho \qquad (2)$$

where $W_o$ and $\rho$ are the initial sample weight and the density of the carbon respectively. Since rigorous interpretation of the rate data is not attempted in this paper, the approximate nature of the surface area calculated from equation (2) is thought to be adequate. The calculated rates per unit area are presented in Figure 2 as ln(rate) vs conversion plots. The data indicate that in both oxygen and carbon dioxide the oxidation rate per unit surface are a decreases in the following order: diamond, graphite, and carbon black. Of the three carbon forms, diamond has the highest packing density, followed by graphite and carbon black in decreasing order of density. Thus, it appears that, at 1273 K, the

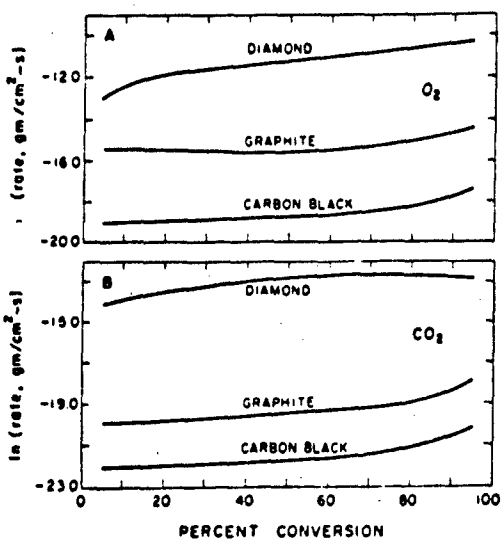


Fig. 2 Reaction rate per unit area vs percent conversion. Reaction Temperature: 1273 K, Gas Flow Rate: 16.7 cc/sec, and Initial Sample Weight: 105 mg.

higher the packing density of carbon, the higher the gasification rate in both oxygen and carbon dioxide. Although the graphite used in these experiments was of very high purity (less than 2 ppm impurity), the diamond powder used in the experiments had some impurities. Semi-quantitative, spectrographic analysis of the diamond powder, performed at Penn State, indicated the presence of 300 ppm of iron, 300 ppm of cobalt and 80 ppm of nickel. These group VIII elements are known to lower the temperature of inception of the gasification reaction and catalyze both the C-$CO_2$ and C-$O_2$ reactions. The high specific reaction rate of diamond is contributed, at least in part, by the presence of these impurities.

At Penn State, carbon black was used as the starting material for the laser assisted synthesis of diamond. Data in figure 2 indicate that if the surface areas of carbon black and diamond were roughly equal, a separation technique based on selective oxidation of carbon black at 1273 K would be unsuccessful. Review of the literature indicates that at temperatures below 970 K, kinetics of reaction of diamond with oxygen is very slow [9]. The results of oxidation tests with both carbon black and diamond powders in air at 773 K are presented in figure 3. The data indicate that carbon black was gasified completely in about four and half hours. However, in this time period, no measurable oxidation of diamond was observed. Thus, it appears that carbon black can be selectively oxidized in air at 773 K from its mixture with diamond. Figure 3 also shows the oxidation curve of a laser treated carbon black sample. The sample contained diamond, chaoite, graphite and carbon black. There is no simple way to determine, in a quantitative manner, the concentrations of various carbon forms in the laser treated material [4]. For this sample, the oxidation curve reached a plateau after 80% conversion. No significant loss in the weight of the sample was observed after this period even after prolonged exposure. After oxidation, the sum total of the weights of diamond, chaoite and graphite together with a small amount of unreacted carbon black was roughly equal to about 20% of the weight of the laser processed sample prior to oxidation.

Although the data presented in this short paper indicate that carbon black can be selectively oxidized in air at 773K from its mixture with diamond, an enormous range of important questions remain unanswered. What is the effect of temperature on the reactivity of diamond? What is the role of the type of reactant gas on the separation of the various carbon forms? Can the selective reaction process be expedited while retaining its efficiency? The current work at Penn State is aimed at addressing some of these questions.

*Acknowledgements* - Financial support for this work was provided by the office of Naval Research.

*Materials Research Laboratory* M. ALAM
*The Pennsylvania State University* T. DEBROY
*University Park, PA 16802* R. ROY

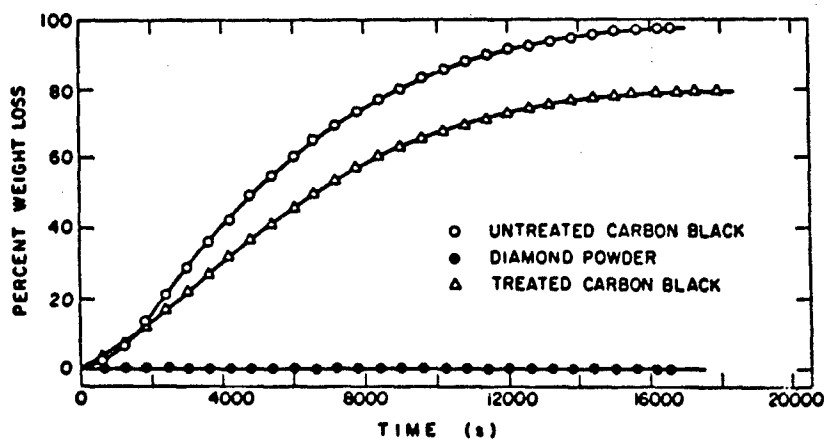


Fig. 3 Percent weight loss vs time plots for oxidation in air at 773 K. Gas Flow Rate: 13.3 cc/sec, and Initial Sample Weight: 105 mg.

## REFERENCES


1. F.P. Bundy, H.M. Strong and R.H. Wentorf, Jr., *Chemistry and Physics of Carbon*, (eds.) P.L. Walker, Jr. and P.A. Thrower, Marcel Dekker, New York, **10**, 213 (1973).
2. D.V. Fedoseev, V.L. Bukhovest, I.G. Vershavskaya, A.V. Lavrent'ev and B.V. Derjaguin, *Carbon*, **21**, 237 (1983).
3. D.V. Fedoseev, I.G. Vershavskaya, A.V. Lavrent'ev and B.V. Derjaguin, *Powder Technology*, **44**, 125 (1985).
4. M. Alam, T. DebRoy, and R. Roy, Diamond Formation in Air by the Derjaguin Laser Process, submitted for publication.
5. M. Alam, T. DebRoy and R. Roy, High Pressure Phases of $SiO_2$ made in Air by Derjaguin Laser Process, unpublished documentation, Department of Materials Science and Engineering, Penn State University.
6. J.C. Angus, H.A. Will and W.S. Stanko, *J. Appl. Phys.*, **39**(6), 2915 (1968).
7. P.S. DeCarli and J.C. Jamieson, *Science*, **133**, 1821 (1961).
8. O. Levenspiel, *Chemical Reaction Engineering*, 368, John Wiley and Sons, New York, 1972.
9. A.K. Holliday, G. Hughes and S.M. Walker, *Comprehensive Inorganic Chemistry*, (eds.) J.C. Bailar, H.J. Emeleus, Sir Ronald Nyholm and A.F. Trotman-Dickenson, Pergamon Press, Oxford, **1**, 1197 (1973).

journal

Reprinted from the Journal of the American Ceramic Society, Vol. 73, No. 3, 1990

J. Am. Ceram. Soc., 73 [3] 733–35 (1990)

# Laser-Induced Calcite–Aragonite Transition

Mansoor Alam,* Tarasankar DebRoy, and Rustum Roy*

Materials Research Laboratory, The Pennsylvania State University, University Park, Pennsylvania 16802

**High-pressure phases of $CaCO_3$ namely aragonite, calcite II, and possibly calcite III, were synthesized in air by exposing 10- to 20-μm-size particles of $CaCO_3$ (calcite I phase) to a $CO_2$ laser radiation at short pulse lengths (≤0.1 ms). The process, therefore, has the same effect as exposing the particles to at least several hundred megapascals pressure. Processing at higher pulse lengths resulted in the decomposition of $CaCO_3$ to CaO and $CO_2$. The extent of decomposition increased with increasing pulse length. [Key words: calcite, phase transformations, processing, lasers, decomposition.]**

## I. Introduction

The calcite–aragonite relationship is one of the most interesting phase transitions from the geochemist's viewpoint. Although the equilibrium phase relations are now generally accepted with calcite I as the stable phase near earth-surface ambients and aragonite stable[1] only above about $3.5 \times 10^8$ Pa (3.5 kbar) at 25°C, the early and common formation of aragonite in huge amounts in many marine $CaCO_3$ rocks, and also in many laboratory experiments, has demanded an explanation. The first of these explanations relied on the solid solution of $Sr^{2+}$ or $Pb^{2+}$ to stabilize the aragonite structure. Although this was both very plausible and supported by the presence of *small* amounts of $Sr^{2+}$ in the samples examined quantitatively, this explanation could not work.[2] Laboratory experiments now point to metastable crystallization of aragonite, possibly epitaxially on a preformed hydrated $MgCO_3$ phase.[3] The calcite to aragonite transition has also been shown by Burns and Bredig[4] and Dachille and Roy[5] to occur in the process of grinding $CaCO_3$. In this study we report a new method to accomplish the same end.

In 1982 and 1985, Fedoseev *et al.* reported[6,7] some most extraordinary findings. They claimed that dropping a stream of fine powder through a laser beam of modest flux intensity would convert graphite to diamond and quartz to coesite and stishovite. This extraordinary result was not widely believed by the scientific community. In 1988 we reported confirmation and extension of the Fedoseev and Derjaguin results,[8,9] showing indeed both that diamond could be so formed and that possibly even more dense polymorphs of $SiO_2$, with $\alpha$-$PbO_2$ and $Fe_2N$ structures could be made by pulsed laser fluxes impinging on $SiO_2$ powders.

The simplest explanation for this effect is that these fine powders absorb the 10.6-μm radiation so fast that both temperature ($T$) and pressure ($p$) are raised very rapidly[6,7] and transition occurs *in the stable p–T regime.* What is not easy to get is any indication of the actual temperatures and, hence, pressures, involved. We selected the calcite–aragonite transition to provide some indications on the $p$–$T$ conditions actually achieved in the laser process. This is possible since two very different reactions are possible with calcite. These are the solid–solid calcite I to aragonite phase transformation and the thermal decomposition of $CaCO_3$ (calcite I) to CaO and $CO_2$. Both reactions are functions of pressure and temperature. The $p$–$T$ equilibria for the two reactions[1] are shown in Figs. 1(A) and (B), although in the latter case it is $CO_2$ pressure.

If the typical pulsed laser exposures generate the high-pressure solid phase, that would indicate the $p$–$T$ conditions shown in Fig. 1(A). On the other hand, if the exposures generate the thermal decomposition products (CaO + $CO_2$), that would indicate the $p$–$T$ conditions shown in Fig. 1(B).

## II. Experimental Procedure

A schematic diagram of the experimental setup is shown in Fig. 2. The setup consisted of a $CO_2$ laser† and electrically

†Everlase model 525, Coherent General, Sturbridge, MA.

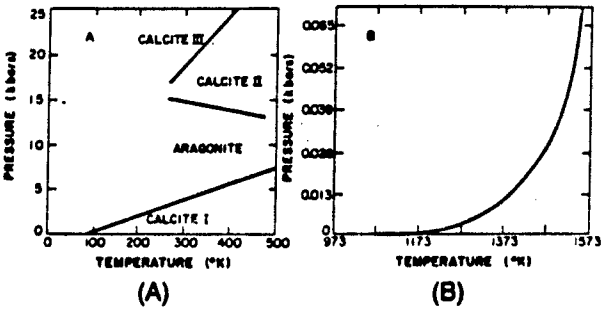


Fig. 1. $p$–$T$ equilibria for (A) $CaCO_3$ system and (B) CaO–$CO_2$ system.

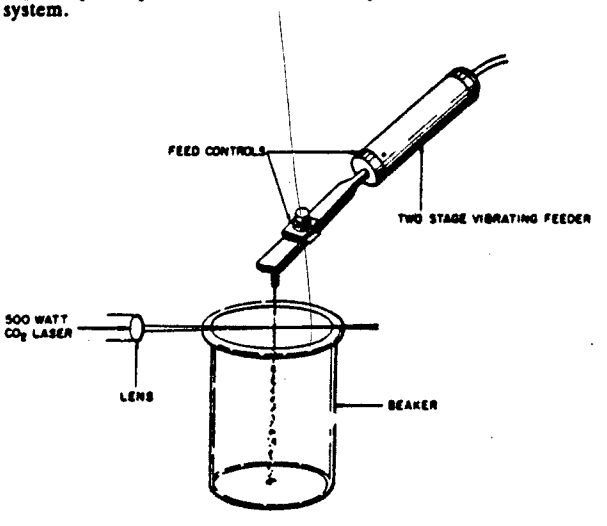


Fig. 2. Schematic of the experimental setup.

V. J. Larsia—contributing editor

Manuscript No. 198261. Received July 12, 1989; approved September 29, 1989.

Supported by the Office of Naval Research and by the Hoechst Celanese Co.

*Member, American Ceramic Society.

*Now with New Mexico Institute of Mining and Technology, Socorro, NM.

**Table I. Experimental Conditions for Processing***

| Sample No. | Pulse length (ms) | Energy/pulse (J) | Transformation |
|---|---|---|---|
| A | 0.01 | 0.01 | Yes |
| B | 0.05 | 0.02 | Yes |
| C | 0.10 | 0.04 | Yes |
| D | 2.00 | 0.50 | No |

*Material: $CaCO_3$ (calcite I); particle size: 10 to 20 μm; purity: >99.7%; atmosphere: air; laser: pulsed $CO_2$; frequency: 50 Hz; number of passes: 10; feed rate: 10 mg/s; and spot size: 0.025 cm.

powered vibrating feeder. The particles were allowed to fall freely and were treated with a horizontally transmitted laser beam. The laser-processed particles were collected in a glass beaker. The type of material used and the specific conditions of the experiments are presented in Table I. After laser processing, the material was characterized by XRD and SEM.

## III. Results and Discussion

Powder XRD patterns of unprocessed and laser-processed samples are shown in Fig. 3. The corresponding interplanar spacing values calculated from the patterns in Fig. 3 are presented in Table II. The data in Fig. 3 and Table II indicate that when calcite I particles are irradiated with pulses of 0.1 ms and less (high heating and cooling rates), they transform to high-pressure polymorphs aragonite, calcite II, and possibly calcite III. At greater pulse length, where more energy is deposited in the material and the heating and cooling rates are relatively low, calcite I particles thermally decompose to CaO and $CO_2$, instead of transforming to high-pressure polymorphs.

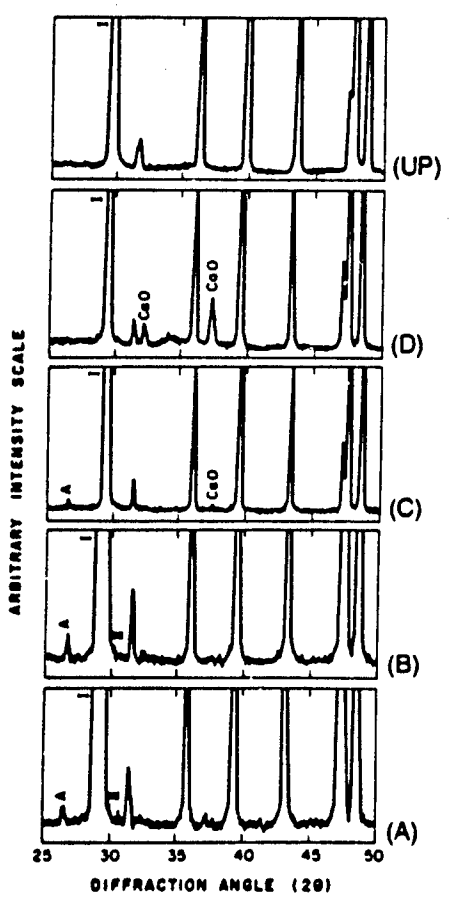


**Fig. 3.** XRD patterns of unprocessed (UP) and laser-processed calcite I samples. Details of the experimental conditions are presented in Table I.

A comparison of the X-ray data for laser-treated sample A with the data for the starting material indicates many new peaks in the processed sample. Ten peaks in this sample can be attributed to aragonite. Of these, four belong exclusively to aragonite and include the first, second, and fourth highest intensity peaks of aragonite. Three more peaks are not common to calcite I but are common either to CaO or to other high-pressure $CaCO_3$ phases. Furthermore, seven peaks in this sample can be attributed to the calcite II phase. One of the peaks belongs exclusively to calcite II and is the 100-intensity peak of calcite II. Three other peaks are not common to calcite I but belong either to CaO or to other high-pressure $CaCO_3$ phases indicated in Table II. Also in this sample, seven peaks can be attributed to the calcite III phase. Of these, two low-intensity peaks at $2.65 \times 10^{-1}$ and $2.53 \times 10^{-1}$ nm (2.65 and 2.53 Å) belong exclusively to calcite III. Of the remainder, three are common to calcite I and two others are common to other high-pressure phases. Of the two 100 intensity peaks of calcite III, one at $3.06 \times 10^{-1}$ nm (3.06 Å) is present, but is common to calcite. Therefore, the analysis of X-ray data suggests that both aragonite and calcite II phases are present. Calcite III may also be present, although the evidence for this phase is not conclusive: Examination of the X-ray data for sample B, where the pulse length and the energy deposition were increased, indicates that even at 0.05-ms pulse length, the presence of aragonite and calcite II can be confirmed.

When the pulse length is increased to 0.1 ms, the decomposition of $CaCO_3$ begins alongside the formation of aragonite. This can be observed from the X-ray data for sample C, which shows four new peaks. Of these, the peak at $2.40 \times 10^{-1}$ nm (2.40 Å) can be attributed to the 100-intensity peak of CaO. The peak at $1.83 \times 10^{-1}$ nm (1.83 Å) can be attributed to vaterite, still another $CaCO_3$ phase. The two other new peaks at $3.36 \times 10^{-1}$ and $2.32 \times 10^{-1}$ nm (3.36 and 2.32 Å) can be attributed to 100- and 30-intensity peaks of aragonite. Thus, aragonite is present in this sample together with calcite I and its decomposition product CaO.

In sample D, the pulse length and energy deposited is significantly increased compared with all the previous samples (A, B, and C). Because of "slow" heating and cooling rates, the laser treatment does not result in the generation of high-pressure phases in quantities significant enough to be detected by XRD. Instead, calcite I decomposes to CaO. The X-ray data shows two new peaks at $2.78 \times 10^{-1}$ and $2.41 \times 10^{-1}$ nm (2.78 and 2.41 Å), both of which can be attributed to prominent peaks of CaO. Furthermore, unlike all other samples, the 100-intensity peak of aragonite is absent in this sample. Thus at 2-ms pulse length, high-pressure phases cannot be detected, and the $p$–$T$ trajectory of the sample has placed it completely in the CaO–$CO_2$ stability region. At shorter pulse lengths where there has been phase transformation to aragonite and calcite II, the $p$–$T$ conditions actually achieved are those presented in Fig. 1(A).

The morphology of untreated and laser-treated $CaCO_3$ particles is shown in Fig. 4. It appears that calcite I particles did not undergo significant morphological changes because of laser irradiation, and that the reaction is a direct solid-state transformation.

The spectrographic analysis of the starting material and laser-processed sample indicates that no foreign material was introduced during the experiments.

## IV. Conclusions

This study shows that irradiation of 10- to 20-μm-size particles of $CaCO_3$ (calcite I) by a pulsed $CO_2$ laser beam results in two competing processes, phase transformation and thermal decomposition. At pulse lengths lower than 0.1 ms, calcite I particles undergo transformation to high-pressure

Table II. Powder XRD Patterns of Unprocessed and Laser-Processed Calcite I Samples

| d spacings ($\times 10^{-1}$ nm (Å)) | | | | | |
|---|---|---|---|---|---|
| Unprocessed sample | Sample A | Sample B | Sample C | Sample D | Pertaining to the $CaCO_3$ phase (from Powder Diffraction File*) |
| | 3.36 | 3.36 | 3.36 | | Aragonite (3.396/100) |
| 3.03 | 3.06 | 3.07 | 3.05 | 3.04 | Calcite I (3.035/100), calcite III (3.02/100) |
| | 2.98 | 2.99 | | | Calcite III (2.998/100) |
| | 2.91 | | | | ? |
| 2.84 | 2.84 | 2.84 | 2.84 | 2.84 | Calcite I (2.845/3) |
| | 2.79 | 2.78 | | 2.78 | Calcite II (2.793/3), CaO (2.778/34) |
| | 2.70 | 2.70 | | | Aragonite (2.70/46) |
| | 2.65 | 2.64 | | | Calcite III (2.65/6) |
| | 2.62 | | | | $CaO_4$ (2.63/80) |
| | 2.52 | 2.53 | | | Calcite III (2.53/10) |
| 2.49 | 2.49 | 2.49 | 2.50 | 2.50 | Calcite I (2.495/14), aragonite (2.481/33), calcite II (2.47/15) |
| | 2.40 | 2.40 | 2.40 | 2.41 | Aragonite (2.409/14), CaO (2.405/100) |
| | 2.37 | 2.36 | | | Aragonite (2.372/38), calcite III (2.37/16) |
| | 2.34 | 2.32 | 2.32 | | Aragonite (2.341/31), vaterite (2.318/5) |
| 2.28 | 2.28 | 2.29 | 2.29 | 2.29 | Calcite I (2.285/31), calcite II (2.264/20), calcite III (2.28/10), vaterite (2.282/2) |
| | 2.19 | | | | Aragonite (2.188/11) |
| | | 2.13 | | | Calcite II (2.113/2), vaterite (2.113/20) |
| 2.09 | 2.10 | 2.10 | 2.10 | 2.10 | Calcite I (2.095/28), aragonite (2.106/23) |
| | 2.06 | 2.04 | | | Calcite II (2.064/20), calcite III (2.08/6), vaterite (2.063/60) |
| | 1.97 | 1.97 | | | Aragonite (1.977/65) |
| | | 1.96 | | | Calcite II (1.954/5), $CaO_4$ (1.95/30) |
| 1.92 | 1.94 | 1.94 | 1.93 | 1.93 | Calcite I (1.927/5) |
| 1.91 | 1.92 | 1.92 | 1.91 | 1.91 | Calcite I (1.913/17) |
| 1.88 | 1.88 | 1.88 | 1.88 | 1.88 | Calcite I (1.875/17), aragonite (1.877/25), calcite II (1.886/20), calcite III (1.88/2) |
| | 1.85 | 1.86 | | | Vaterite (1.854/30), calcite II (1.869/20) |
| | | 1.84 | 1.83 | | Vaterite (1.82/70) |

*Joint Committee on Powder Diffraction Standards, International Center for Diffraction Data, Swarthmore, PA.

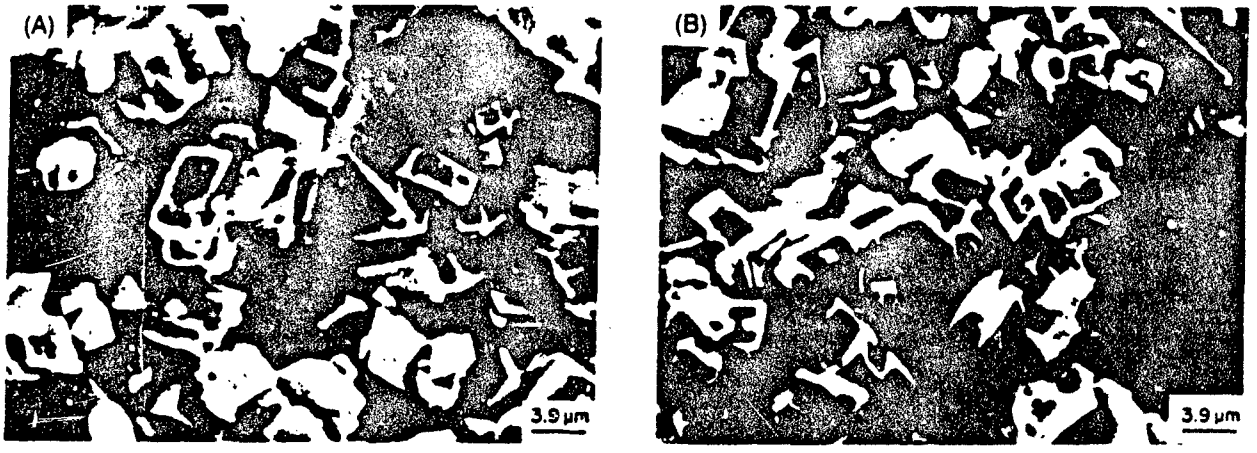


Fig. 4. SEM photographs of (A) unprocessed and (B) laser-processed sample B.

polymorphs aragonite and calcite II and possibly calcite III. At greater pulse lengths, calcite I particles decompose to CaO and $CO_2$. The extent of the decomposition increases with increasing pulse length. The morphology and size of calcite I particles do not change significantly because of the laser treatment.

## References


[1]E. M. Levin, C. R. Robbins, and H. F. McMurdie, Phase Diagrams for Ceramists, 1964. Edited by M. K. Reser. American Ceramic Society, Columbus, OH; Fig. 321.

[2]G. J. F. Macdonald, "Experimental Determination of Calcite-Aragonite Equilibrium Relations at Elevated Temperatures and Pressures," *Am. Mineral.*, 41, 744–56 (1956).

[3]J. W. McCauley and R. Roy, "Controlled Nucleation and Crystal Growth of Various $CaCO_3$ Phases by the Silica Gel Technique," *Am. Mineral.*, 59, 947–63 (1974).

[4]J. H. Burns and M. A. Bredig, "Transformation of Calcite to Aragonite by Grinding," *J. Chem. Phys.*, 25, 1281 (1956).

[5]F. Dachille and R. Roy, "High-Pressure Phase Transformations in Laboratory Mechanical Mixers and Mortars," *Nature (London)*, 186, 34, 71 (1960).

[6]D. V. Fedoseev, V. L. Bukhovets, I. G. Varshavskaya, A. V. Lavrent'ev, and B. V. Derjaguin, "Transition of Graphite into Diamond in a Solid Phase Under the Atmospheric Pressure," *Carbon*, 21, 237–41 (1983).

[7]D. V. Fedoseev, I. G. Varshavskaya, A. V. Lavrent'ev, and B. V. Derjaguin, "Phase Transformations in Highly Disperse Powders During Their Rapid Heating and Cooling," *Powder Technol.*, 44, 125–29 (1985).

[8]M. Alam, T. DebRoy, R. Roy, and E. Breval, "High-Pressure Phases of $SiO_2$ Made in Air by Fedoseev–Derjaguin Laser Process," *Appl. Phys. Lett.*, 53 [18] 1687–89 (1988).

[9]M. Alam, T. DebRoy, R. Roy, and E. Breval, "Diamond Formation in Air by the Fedoseev–Derjaguin Laser Process," *Carbon*, 27 [2] 289–94 (1989).

# $B_2O_3$: Phases Present at High Pressure and Temperature

Varanasi Srikanth, Rustum Roy, Earl K. Graham, Donald E. Voigt

Materials Research Laboratory
The Pennsylvania State University
University Park, Pennsylvania 16802

Revised: 11 September, 1991

## Abstract

Boron suboxide compounds are of interest because of their low densities coupled with high hardness. In the present study, we have attempted to determine the nature of the $B_xO$ phases that occur in the field defined by pressures of zero to 1.5 GPa, temperature between 1200 and 1700°C, and the compositional range $\frac{2}{3} \leq x \leq 24$. Amorphous boron powder and boric acid $B_2O_3$ were the starting reactants for all the runs. The processing of the specimens was carried out in a controlled atmosphere furnace, a hot pressing assembly and in a piston-cylinder high pressure apparatus within quasi-hydrostatic and inductively heated cell assemblies. After processing at elevated temperature and pressure, for compositions over the range $\frac{2}{3} \leq x \leq 6$, $B_2O_3$ (identical to the hexagonal starting material) and $B_6O$ ($R\bar{3}m$) were the dominant phases present. For the compositions $6 \leq x \leq 24$, $B_6O$ and rhombohedral B were the primary phases identified. In general, the hardness of the processed composites was dominated by the occurrence of $B_6O$ (approximately equivalent to $B_4C$). However, there is some suggestion of particularly high values of hardness on a very localized scale in specimens near the $B_{22}O$ composition.

Boron compounds are characterized by unique bonding and crystal structure properties that give rise to a variety of interesting and useful materials.[1] Their strong and short covalent bonding provides the basis for a wide range of distinctive refractory, thermoelectric, and optical properties. Boron suboxides, in particular, have been of interest for a number of years because of their low densities coupled with exceptional hardness properties.[2]

Previous work on boron suboxide ($B_xO$ with $1 \leq x \leq \infty$) compounds generally has focused on the specific stoichiometries $B_2O_3$, $B_2O$, and $B_6O$. In the case of $B_2O_3$, Dachille and Roy[3] demonstrated the occurrence of a crystalline high pressure phase above about 2.2 GPa at 400°C. Nine XRD lines were identified distinctly different from those of the low pressure hexagonal $B_2O_3$ initial phase, but the data were insufficient to define the crystal structure of the high pressure material or any characteristic physical properties. Stoichiometric high pressure-temperature phases of $B_2O$ have been prepared and described by Hall and Compton[4] and Endo et al.[5] In the former study, a graphite-like $B_2O$ compound was synthesized by the reduction of $B_2O_3$ with B or Li and by the oxidation of B with $KClO_3$. The preparation was carried out within the pressure and temperature ranges of 5.0 to 7.5 GPa and 1200 to 1800°C. The $B_2O$ synthesis of Endo et al. was carried out by reacting BP with oxygen derived from the thermal decomposition of $CrO_3$ to $CrO_2$ at pressures of 3.5 to 5.5 GPa in the temperature range 1000 to 1200°C. The recovered $B_2O$ high pressure phase appeared to have a diamond-like structure and was characterized by a Vickers microhardness (100 gm load) of 40.5 GPa.

Stoichiometric $B_6O$ with a hexagonal structure was synthesized by Rizzo et al.[6] by reaction hot-pressing $B_2O_3$ and B at 1300-1400°C. The polycrystalline aggregates produced had Vickers hardness (100 gm load) values up to 37.4 GPa. Later work[7] demonstrated that $B_6O$ could be synthesized at ambient temperature under a pressure of 11.0 GPa, or at 6.0 GPa and 1000°C. In an extensive study of $B_6O$, produced by reaction hot-pressing $B_2O_3$ and B at 1900-2000°C, Petrak et al.[2] assigned it to space group $R\bar{3}m$ (formula $B_{12}O_2$) and calculated a density of 2.602 gm/cm$^3$. Later work[8] by the same group revealed $B_6O$ aggregate Knoop microhardness values similar to $B_4C$ and even higher. Petrak et al.[2] also studied the phases present in hot-pressed specimens of $B_xO$ over the compositional range $5 \leq x \leq 8$. In

all runs the dominant phase was rhomobohedral $B_6O$, with secondary $B_2O_3$ for x=5 and B for x=7 and 8.

In a study by Badzian, carried out in Poland in cooperation with this laboratory, B-O specimens very rich in B were made and noted as being very hard. In 1987 Badzian et al.[9] reported diamond-like hardness, as demonstrated by contact scratch and wear experiments. Chemical analysis of Badzian's specimen by SIMS and AES indicated an oxygen level of 4-5%, suggesting a stoichiometry near $B_{22}O$. Considering the favorable crystal chemical characteristics, and the promising structure and mechanical property results from the foregoing studies, it is surprising that so little is known about the phase relations of $B_xO$ compounds in general. In particular, there has been no systematic effort to define and characterize the phases present in the ambient to moderate P, T field over an extended range of composition X. For this reason, the present study was conducted to determine the nature of the $B_xO$ phases that occur within the field defined by 0 to 1.5 GPa, 1200 to 1700°C, and $\frac{1}{6} \leq x \leq 24$.

Experimental Procedure

The starting materials for all of the processed specimens consisted of amorphous boron powder (CERAC, Inc.; 99.9+% purity; 0.3 $\mu$m average particle size)* and boric acid $B_2O_3$ (CERAC, Inc.; 99.9+% purity; 75$\mu$m average particle size). These components were mixed in the appropriate mass ratios in a paint shaker with plastic spheres for two hours.

Three different preparation methods were used:

(a) Sintering in argon atmosphere. Sintering in an argon atmosphere was carried out in a tubular furnace with a hot zone 25 cm long at 1700°C. Boron suboxide green compacts were placed at the center of the hot zone of the furnace. The specimens were exposed to flowing argon gas until the sintering cycle was complete. The heating rate of the furnace was kept at 5°C/min until the required sintering temperature (1500°C or 1700°C) was reached, at which point the specimens were processed for six hours and then cooled at a rate of 10°C/min to room temperature.

(b) Uniaxial hot pressing. Several samples were prepared by reaction hot pressing at 1700°C and 0.020 GPa in a laboratory hot press (Advanced Vacuum Systems)** using a graphite die with

graphite rams. The hot pressing temperature was measured using an optical pyrometer. An intermediate boron nitride layer was provided between the graphite rams and the sample. Pressure was applied to the graphite rams after the assembly reached 1000°C. Prior to starting the run a vacuum was created in the system.

(c) High-pressure processing. An additional set of specimens was prepared by processing sintered pellets of the desired $B_xO$ stoichiometry at high pressure and temperature in a piston-cylinder apparatus.[10] The mixed starting materials were initially compacted at 0.014 GPa in a cylindrical steel die at ambient temperature, yielding aggregate pellet specimens 12 mm in diameter and 6 mm high. This step was followed by sintering at a temperature of 1500 to 1700°C for several hours in a flowing Argon atmosphere. The phases present in the pre-processed sintered pellets were identified by surface scattered XRD data.

The piston-cylinder apparatus and specific high-pressure cell used in our experiments (with slight modifications) was developed and described previously by Baker and Eggler.[11] The cylindrical high-pressure cells consisted of outer talc and pyrophyllite sleeves separated from the $B_xO$ pellet specimens by an inner pyrex liner to inhibit reaction from fluids derived from dehydration at high temperature. Heating was achieved by a graphite furnace sleeve inserted directly inside the pyrex liner. The specimen was isolated from the heater assembly by BN powder and crushable alumina spacer material. The temperature of the specimen was monitored by a Type S Pt-$Pt_{90}Rh_{10}$ thermocouple inserted through the steel base-plate of the high-pressure cell into the alumina directly adjacent to the $B_xO$ pellet.

The processing procedure was developed in such a manner as to minimize fracture and fragmentation in the final prepared specimen. Unfortunately, because of this constraint, a rapid quench was not possible. The following method seemed to provide the most favorable specimens. (1) Pressure and temperature were simultaneously increased linearly until the desired conditions were reached. This step was accomplished in about five minutes. (2) Pressure and temperature were maintained at a constant level for the period of time selected for the run (generally 30 to 120 minutes). (3) Finally, pressure was dropped at a constant temperature until contact with the furnace was broken, whereupon

both P and T were dropped simultaneously. This last step generally provided coherent specimens, but at the possible expense of retaining metastable high pressure phases.

After removal from the piston-cylinder apparatus and high-pressure cell, the processed specimens consisted of irregular disks about 10 mm in diameter and 5 mm in thickness. They were usually characterized by a thin greyish-black skin (possible BN contamination) and a mottled brown-red interior. Some minor (radial and longitudinal) cracks were often present.

Analysis of the Processed Specimen Products: Phases Present

The phases present in the processed specimens were identified by surface scattered and powder XRD measurements. Diffraction angles and line intensities were compared to all boron compounds in the compositional area listings in the ASTM files. The summary results for the compositional range and pressure-temperature conditions chosen for processing are shown in Table 1. As indicated in the table, only three phases were consistently recognized over the pressure (zero to 1.0 GPa), temperature (ambient to 1700°C), and compositional ($\frac{2}{3} \leq x \leq 24$) range of our experiments: (1) $B_2O_3$ (the hexagonal low pressure phase identical to the starting material); (2) $B_6O$ (as recognized and defined by previous investigators[2, 6-8]); and (3) rhombohedral B. For the compositions $\frac{2}{3} \leq x \leq 6$, $B_2O_3$ and $B_6O$ are the dominant phases present, their relative proportions defined by the mixture stoichiometry. Over the range $6 \leq x \leq 24$, $B_6O$ and rhombohedral B are the prevailing materials, with the latter dominating as x approaches higher values. These same relationships defined the ambient pressure (1700°C) runs, as well as those carried out at 1.0 GPa (1350°C) and above.

Preliminary Property Measurements

As part of our standard processed specimen analysis procedure, bulk density was measured by the Archimedes method, as well as porosity. The densities were variable, but generally reflected the nature of the mixture and extent of porosity. For example, in the case of the $B_{22}O$ specimens, $\rho_B$ varied between 2.20 and 2.46 gm/cm$^3$, but was usually close to the latter. This range is consistent with the XRD results, which indicate a mixture of $B_6O$ ($\rho_B$=2.60 gm/cm$^3$) and rhombohedral B ($\rho_B$=2.29 gm/cm$^3$), plus some porosity. Specifically, for an ideal (zero porosity) mixture of $B_6O$ and B of $B_{22}O$

stoichiometry, $\rho_B = 2.52$ gm/cm$^3$. Porosities of one to four percent (typical of our specimens) would, therefore, yield bulk densities in the range 2.42 to 2.50 gm/cm$^3$. The presence of unreacted $B_2O_3$ in the specimens also would tend to produce somewhat lower bulk density than expected.

Our original intent was to also describe the elastic and hardness properties of the processed $B_xO$ specimens. Unfortunately, the inhomogeneous nature of our processed specimens, and the frequent occurrence of structure microcracks, precluded a definitive measurement of the elastic moduli by the ultrasonic technique at our disposal. Moreover, the same specimen problems made it difficult to obtain systematic and consistent hardness values. Interest in the hardness of these materials was very high due to the observation by Badzian of scratches in the [100] face of natural diamond by a melted specimen near the $B_{22}O$ composition. Attempts to repeat the scratching experiments with our high-pressure processed specimens gave inconsistent results. Occasionally similar scratches seemed to be present on the diamond face (Fig. 1). A second more consistent observation was that grinding the surface (using diamond paste thinned with mineral oil) appeared to cause some sort of phase change or nanoscale disintegration. Fragments of processed specimen material containing $B_6O$ (see Table I) invariably were observed to scratch $Al_2O_3$ (easily), and SiC. These results were corroborated for one of our $B_{22}O$ specimens sent to F. Corrigan at the General Electric Company. Scratch and Knoop hardness tests (1000 gm indenter load) indicated that the $B_{22}O$ specimen exceeded both sapphire and silicon carbide, but was not as hard as (and was scratched by) BZN 8000 compact and DCBN. Tests in comparison to boron carbide were inconclusive. This latter observation is consistent with the Knoop microhardness results of Petrak et al.[8] for $B_6O$ and $B_4C$, who reported values of 29.8±1.5 GPa and 29.6±1.3 GPa, respectively. In turn, this result supports our compositional analyses (Table I), which indicate that $B_6O$ is a major phase in the $B_xO$ specimens for which $x > 5$.

Additional specimens of $B_{22}O$ were provided to T.P. Weihs at the University of Oxford in order to evaluate very localized hardness values using a nanoindenter apparatus. Their differential method, which senses the depth of indentation as a function of the applied load, has been shown[12] to yield the plastic hardness and elastic modulus of volumes a few hundred nm in cross section. At the smallest scale,

even inherent atomic lattice properties can be observed. Thirty-nine separate nanoindentation tests were performed on the boron oxide specimen with mixed results. The initial nine tests were carried out with a sharp indenter tip and yielded very high nanohardness values (in the range 70 to 146 GPa). However, because the analysis of the technique is based on a flat punch contacting an elastic half-space, a second set of tests (thirty) were conducted with an indenter tip slightly rounded by grinding. The results for the blunted tip were over an order of magnitude less, with hardness values in the range 0.8 to 6.9 GPa.

The reasons for the foregoing discrepancies and anomalous behavior in the hardness of $B_{22}O$ are not clear. The standard microhardness measurements indicate a value of about 30 GPa, which is reasonably consistent with a primary compositional mixture of $B_6O$ and rhombohedral B, as defined by the XRD results. However, there remains some suggestion that the material is characterized by, perhaps, very small scale features of extremely high hardness. More definitive experiments are necessary to confirm and understand the nature of these observations.

Our foregoing results are consistent with the hot-pressed (P=0.04 GPa; T=1900-2000°C) specimens of Petrak et al.[2] over the limited compositional range $5 \leq x \leq 8$. We have demonstrated that the same phases persist out to $\frac{5}{6} \leq x \leq 24$, and up to 1.0 GPa in pressure. However, our pressure range was insufficient to synthesize the high pressure phases induced in $B_2O_3$ by Dachille and Roy[3] and $B_2O$ by Hall and Compton[4] (graphite) and Endo et al.[5] (diamond-like), which appear to require levels in excess of 2.2 GPa. Our observation that $B_6O$ appears to be stable at 1.0 GPa and 1350°C is consistent with the ambient pressure results of Rizzo et al.[6] and the static compression data of Zubova and Burdina.[7] The collective results suggest that the stability field of hexagonal $B_6O$, relative to $B_2O_3$ + B, decreases in temperature as pressure increases.

Acknowledgments: Support for this research was provided by the Office of Naval Research (Grant No. N00014-86-K-0238). We are grateful to F. Corrigan of the General Electric Company and T.P. Weihs of the University of Oxford for their help in the hardness characterization of the $B_{22}O$ specimens. We would also like to thank D.H. Eggler of the Department of Geosciences at Penn State for the use of the high-pressure facilities under his direction.

* CERAC, Inc., P.O. Box 1178, Milwaukee, WI 53201
** Advanced Vacuum Systems, 2 Gill St., Woburn, MA 02139

References

1) D. Emin, "Icosahedral Boron-Rich Solids, "Phys. Today, 55-62, January (1987).

2) D.R. Petrak, R. Ruh, and B.F. Goosey, "Preparation and Characterization of Boron Suboxide," N.B.S. Spec. Publ. 364, Proc. 5th Mat. Res. Symp., 605-611 (1972).

3) F. Dachille, and R. Roy, "A new High-Pressure Form of $B_2O_3$ and Inferences on Cation Coordination from Infrared Spectroscopy," J. Am. Ceram. Soc., 42 [2] 78-80 (1959).

4) T. Hall, and L.A. Compton, "Group IV Analogs and High Pressure, High Temperature Synthesis of $B_2O$," Inorganic Chem., 4 [8] 1213-1216 (1965).

5) T. Endo, T. Sato, and M. Shimada, "High-Pressure Synthesis of $B_2O$ with Diamond-like Structure," J. Mater. Sci. Lett., 6, 683-685 (1987).

6) H.F. Rizzo, W.C. Simmons, and H.O. Bielstein, "The Existence and Formation of the Solid $B_6O$, "J. Electrochem. Soc., 109 [11] 1079-1082 (1962).

7) E.V. Zubova, and K.P. Budina, "Synthesis of $B_6O$ at High Pressures, "Sov. Phys. Dokl., 16 [4] 317-318 (1962).

8) D.R. Petrak, R. Ruh, and G.R. Atkins, "Mechanical Properties of Hot-Pressed Boron Suboxide and Boron," Am. Ceram. Soc., 53 [8] 569-573 (1974).

9) A.R. Badzian, "Superhard Material Comparable in Hardness to Diamond," Appl. Phys. Lett., 53 [25] 2495-2497 (1988).

10) F.R. Boyd, and J.L. England, "Apparatus for Phase-Equilibrium Measurements at Pressures Up to 50 Kilobars and Temperatures Up to 1750°C, J. Geophys. Res., 65, 741-748 (1960).

11) D.C. Baker, and D.H. Eggler, "Fractional Paths of Atka (Aleutians) High-Alumina Basalts: Constraints from Phase Relations, "J. Volcan. Geotherm. Res., 18, 387-404 (1983).

12) J.P. Pethica, and W.C. Oliver, "Mechanical Properties of Nanometer volumes of Material: Use of the Elastic Response of Small Area Indentations," preprint of a paper to be published (1991).

Table I. Phases Present in the Boron Suboxide Specimens Synthesized in the Pressure-Temperature Runs

| Bulk Nominal Mixture | P = Ambient<br>T = 1700 °C | P = 1.0 GPa<br>T = 1350 °C |
|---|---|---|
| $B_2O_3$ | $B_2O_3$ | $B_2O_3$ |
| $B_2O$ | $B_2O_3 + B_6O$ | $B_2O_3 + B_6O$ |
| $B_4O$ | $B_2O_3 + B_6O$ | $B_2O_3 + B_6O$ |
| $B_6O$ | $B_6O$ | $B_6O$ |
| $B_8O$ | $B_6O + B$ | $B_6O + B$ |
| $B_xO$[a] | $B_6O + B$ | $B_6O + B$ |
| $B_{22}O$[b] | $B_6O + B$ | $B_6O + B$ |
| $B_{24}O$ | $B + B_6O$ | $B + B_6O$ |

[a] Range: $10 \leq x \leq 20$ (in increments of $x = 2$).
[b] Run also made at 1.5 GPa with same results.

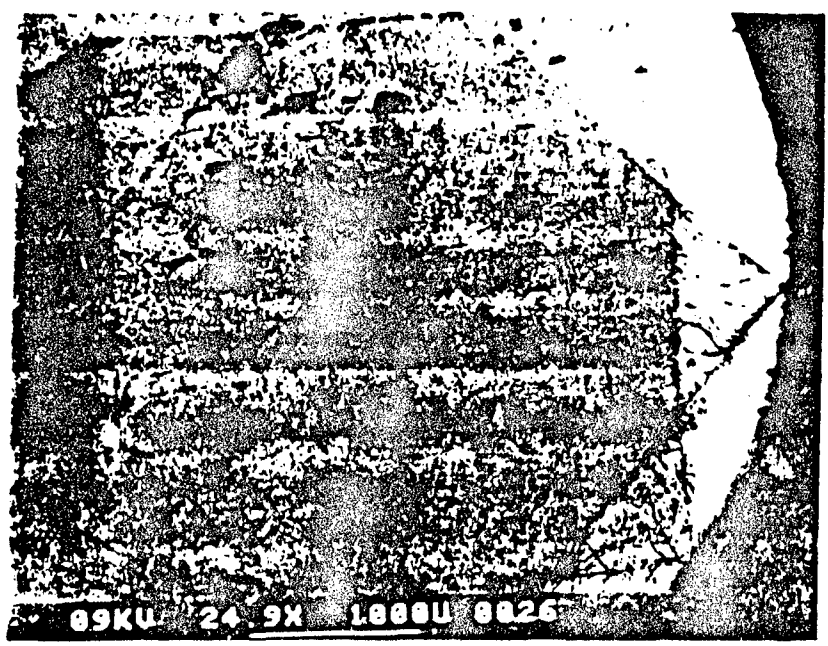


Figure 1. SEM of [100] face of single-crystal diamond after contact abrasion with $B_{12}O$ specimen and etch treatment with hot nitric acid.